

Influence of the spin-orbit split-off valence band on the hole g factor in semiconductor nanocrystals

M. A. Semina ^{*}, A. A. Golovatenko , and A. V. Rodina
Ioffe Institute, 194021, St.-Petersburg, Russia

 (Received 15 September 2021; accepted 1 November 2021; published 18 November 2021)

We present results of $\mathbf{k} \cdot \mathbf{p}$ calculations of the effective g factor of holes confined in spherical, cube, and planar semiconductor nanocrystals (NCs). We use the six-band Luttinger model for semiconductors with the zinc-blende crystal structure and study the size dependence of the Γ_8 top valence subband hole g factor caused by the admixture of the spin-orbit split-off valence subband Γ_7 . We present semianalytical expressions for the hole g factor which depends on the light- to heavy-hole effective mass ratio β and on the ratio between spin-orbit energy splitting of valence band Δ_{SO} and the hole quantization energy E_h . The admixture of Γ_7 states is significant for small Δ_{SO}/E_h and, in spherical and cube NCs, leads to a strong size dependence of the hole g factor. In thin planar nanoplatelets (NPLs) with infinite or large lateral sizes, the dependence of the heavy-hole g factor on NPL thickness is relatively weak. It is drastically enhanced and may become nonmonotonic in NPLs with finite in-plane sizes due to the additional hole states mixing. We discuss our results in comparison with published experimental data for CdSe- and InP-based spherical NCs and NPLs and point out the specificity of extracting hole g factor from the data measured on excitons.

DOI: [10.1103/PhysRevB.104.205423](https://doi.org/10.1103/PhysRevB.104.205423)

I. INTRODUCTION

Since their discovery four decades ago, semiconductor nanocrystals (NCs) have become the most studied among nanoscale semiconductors [1]. By now, their synthesis by colloidal chemistry has passed into the state of mature technology and provides precise control over the size, shape, and composition [2–4]. Today, a wide area of NCs application includes solar cells, displays, photodetectors, and molecular sensors [5–11]. All these applications are mostly based on the emission or absorption of light by spatially confined electron-hole pairs. Control over the spin state of localized carriers is important for the promising application of NCs in spintronics and quantum computing devices [12–16] and requires among other the knowledge about their g factors.

The g factor (Lande factor) determines the response of electrons, holes, or their complexes to the external magnetic field including the Zeeman energy splitting between spin sublevels and the Larmor frequency of the spin precession. Comprehensive experimental and theoretical studies are being performed in this direction. Using different magneto-optical techniques g factors of electrons, holes, and excitons were measured [17–23]. Theoretical understanding of experimental data on the electron g factor in semiconductor nanostructures of different size, shape, and dimensionality were developed within the multiband $\mathbf{k} \cdot \mathbf{p}$ theory [24–27] and the tight-binding method [28–30].

In the low-field regime, the energy splitting of electron states with opposite spin projections on magnetic field direction is linear on magnetic field strength B and is defined by electron effective g factor g_e . The corresponding Zeeman part

of electron Hamiltonian is

$$\widehat{H}_Z^{(e)} = \mu_B g_e (\mathbf{S}_e \mathbf{B}), \quad g_e = \frac{E_{1/2} - E_{-1/2}}{\mu_B B}. \quad (1)$$

Here $\mu_B = \frac{e\hbar}{2m_0c}$ is the Bohr magneton, m_0 is the free-electron mass, $e = |e|$ is the absolute value of electron charge, and $E_{\pm 1/2}$ are energies of states with spin projection $S_{ez} = \pm \frac{1}{2}$ on the magnetic field direction. The scheme of electron energy-level splitting is shown in Fig. 1.

The value of the bulk electron g factor at the bottom of the conduction band in typical semiconductors with the zinc-blende (zb) crystal structure can be calculated within the second-order $\mathbf{k} \cdot \mathbf{p}$ theory. It was first made to account the contributions from the Γ_8 and Γ_7 valence subbands [31] and phenomenologically taking into account the remote conduction band contribution g_{rb} [32]:

$$g_e \approx g_0 + g_{rb} - \frac{2E_p}{3} \left(\frac{1}{E_g} - \frac{1}{E_g + \Delta_{SO}} \right). \quad (2)$$

Here $E_p = 2|\langle X|\hat{p}_x|S\rangle|^2/m_0$ is the Kane energy expressed via the interband momentum matrix element, E_g is the band gap, Δ_{SO} is the spin-orbit splitting of the valence band. In most cases, g_{rb} can be treated as a fitting parameter in order to obtain the experimental value of g_e , if parameters E_p , E_g , and Δ_{SO} are known. In wurtzite (wz) semiconductors the crystal field splits the fourfold-degenerate Γ_8 valence subband into two twofold-degenerate Γ_9 and Γ_7 subbands resulting in anisotropy of the electron g factor. If the crystal field energy splitting Δ_{cr} is much smaller than Δ_{SO} and E_g , Eq. (2) still describes the electron g factor in the isotropic approximation.

As it can be seen from Eq. (2), g_e differs from the value of free-electron g factor $g_0 = 2$ [31] due to nonzero Δ_{SO} , and in case $\Delta_{SO}/E_g \rightarrow 0$ we would have $g_e \rightarrow g_0$. In semi-

^{*}semina@mail.ioffe.ru

conductors with parametrically strong spin-orbit coupling the difference can be large and g_e can even change the sign. For example, $g_e = -0.44$ in GaAs [33], $g_e = 0.42$ in zb-CdSe [34], $g_e = 0.68$ in wz-CdSe [35], $g_e = -1.66$ in CdTe [36], and $g_e = 1.2$ in InP [36].

Spatial localization of electrons in nanostructures leads to the renormalization of the g factor and even to its spatial anisotropy [24–27,29,37,38]. The main contribution to the g -factor renormalization comes from the effective renormalization of the band gap: in Eq. (2) one has to change $E_g \rightarrow \tilde{E}_g = E_g + E_e$ with E_e being the electron size quantization energy (for details see Appendix A). In small NCs, where the electron localization length at least in one dimension is about 1–2 nm, the contribution of the valence band to the electron g factor decreases with $\Delta_{SO}/\tilde{E}_g \rightarrow 0$ and $g_e(E_e) \rightarrow g_0$. Importantly, the eight-band $\mathbf{k} \cdot \mathbf{p}$ calculations of the electron g factor in spherical NCs provide a very good agreement with results of the tight-binding calculations from Ref. [29] and allow to describe the experimentally observed electron g -factor size dependence (see Appendix A).

The electron localization leads also to the renormalization of the orbital effective g factor (orbital magnetic momentum) [26,39]. While for electrons the orbital contribution is relatively small, it becomes an important effect for the valence band holes due to the complex valence band structure. As a result, there is a substantial variation of hole g factors between nanostructures and their dependence of the actual type of confining potential [30,40–43].

In most $\mathbf{k} \cdot \mathbf{p}$ calculations of the g factor of a hole from the upper valence band, only the four-band Luttinger model is considered while the impact of the interaction with the conduction band as well as with the spin-orbit split valence band is neglected. As a result, in contrast with electrons, in such an approximation the hole g factor is independent of the nanostructure size [42–44]. However, this result holds true until the hole quantization energy E_h is small enough as compared with Δ_{SO} and E_g . In small colloidal NCs with diameter 2–3 nm, or especially in colloidal nanoplatelets with thickness only 1–2 nm, E_h may first become comparable with Δ_{SO} . In this case $\Delta_{SO}/E_h \rightarrow 0$, so that a strong admixture of the spin-orbit split subband and a consequent change of the hole g factor is to be expected. For quantum wells, the size dependence of the hole g factor was predicted theoretically within the eight-band Kane model [45] and studied experimentally [38,46,47]. The Kane eight-band model was also used to study the hole g -factor height dependence in cylindrical narrow band

gap InAs/InP quantum disks [48]. However, the effect of the spin-orbit split valence band contribution to the hole g factor in general form was not consistently considered.

The aim of this paper is to study the effect of admixture of the spin-orbit split-off Γ_7 valence subband on the g factor of hole from the top valence subband in nanostructures of different shapes and sizes. We consider the six-band Luttinger model for semiconductors with the zinc-blende crystal structure and show that results are applicable to wurtzite semiconductors with $\Delta_{cr} \ll E_h$. Dependencies of the hole g factor on the light- to heavy-hole mass ratio β are calculated for spherical, cubic, and planar NCs with different types and sizes of the confining potential. The size dependencies of the hole g factor in CdSe- and InP-based NCs are calculated and compared with the values obtained within the four-band model.

The rest of the paper is organized as follows: In Sec. II we introduce a Hamiltonian of the hole in an applied magnetic field and discuss existing definitions of the hole g factor. In Sec. III we present the calculation results for the hole g factor in spherical and cube NCs, and discuss the influence of a moderate uniaxial shape anisotropy in spheroidal and cuboid NCs. In Sec. IV the hole g factor in thin, close to two-dimensional (2D) nanoplatelets and platelets with finite lateral sizes is considered.

We compare the results of our calculations with published theoretical and experimental data with special attention paid to the method used for the hole g -factor measurement. In this context we discuss also the Zeeman splitting of different exciton states. We summarize our results in Sec. VI and give the additional details in Appendices A, B, and C.

II. VALENCE BAND HOLE IN THE EXTERNAL MAGNETIC FIELD

A. Definition of the hole g factor

We consider a hole from the Γ_8 valence subband and take into account the admixture of the spin-orbit split-off Γ_7 valence subband. To simplify the further analysis we neglect the cubic symmetry of the crystal lattice resulting in the valence band warping or anisotropy of Δ_{SO} . Then, the holes in the external magnetic field are described by the following Hamiltonian, which we rewrite in the hole representation as the sum of four contributions:

$$\hat{H} = \hat{H}_{6 \times 6} + \hat{H}_Z^{(h)} + \hat{H}_B + V_{\text{ext}}(\mathbf{r}). \quad (3)$$

Here

$$\hat{H}_{6 \times 6} = \frac{\hbar^2}{2m_0} \left[(\gamma_1 + 4\gamma)k^2 - 6\gamma \left(\sum_{\alpha=x,y,z} k_\alpha^2 \hat{I}_\alpha^2 + 2 \sum_{\alpha \neq \beta} \{k_\alpha k_\beta\} \{\hat{I}_\alpha \hat{I}_\beta\} \right) \right] - \frac{1}{3} \Delta_{SO} [(\hat{\mathbf{I}} \hat{\boldsymbol{\sigma}}_h) - 1] \quad (4)$$

is the six-band Luttinger Hamiltonian [49,50] describing the hole kinetic energy in spherical approximation in zero magnetic field in the hole representation. Here γ_1 and $\gamma = (2\gamma_2 + 3\gamma_3)/5$ are Luttinger parameters related to the bulk light-hole $m_{lh} = m_0/(\gamma_1 + 2\gamma)$ and heavy-hole $m_{hh} = m_0/(\gamma_1 - \gamma)$ effective masses, \mathbf{k} is the hole wave vector, $\hat{\mathbf{I}} \equiv \hat{\mathbf{I}}_h$ is the

hole orbital angular momentum operator $I = 1$, $\mathbf{s}_h = 1/2 \hat{\boldsymbol{\sigma}}_h$ is the hole effective spin $\frac{1}{2}$ ($\sigma_{h\alpha}$ the Pauli matrices with $\alpha = x, y, z$), and $\{ab\} = (ab + ba)/2$. In the limit of large spin-orbit interaction $\Delta_{SO} \rightarrow \infty$, the top of the valence band can be described by the four-band Luttinger Hamiltonian [51,52].

Following the classical approach introduced by Luttinger [51], the Zeeman part of the hole Hamiltonian in bulk material $\hat{H}_Z^{(h)}$ in the hole representation has the form

$$\hat{H}_Z^{(h)} = -\mu_B(1 + 3\kappa)(\hat{\mathbf{I}}_h \mathbf{B}) + \frac{1}{2}\mu_B g_0(\hat{\boldsymbol{\sigma}}_h \mathbf{B}), \quad (5)$$

where \mathbf{B} is the external magnetic field, κ is the magnetic Luttinger parameter [51]. In the electron representation kinetic energy Eq. (4) changes sign and instead of $\hat{\mathbf{I}}_h$ one has to take the electron orbital momentum $\hat{\mathbf{I}}_e = -\hat{\mathbf{I}}_h$ and the electron spin operator with the Pauli matrices $\hat{\boldsymbol{\sigma}}_e = -\hat{\boldsymbol{\sigma}}_h$. As a result, in both the electron and hole representations, the relative sign between the Zeeman term (5) and kinetic energy (4) remains the same as a change of representation results in sign inversion of both energy and spins. The operator of the hole internal angular momentum is

$$\mathbf{J} \equiv \mathbf{J}_h = \hat{\mathbf{I}}_h + \frac{1}{2}\hat{\boldsymbol{\sigma}}_h. \quad (6)$$

For the Γ_8 subband $J = \frac{3}{2}$ and for the Γ_7 subband $J = \frac{1}{2}$.

We use the following definition of the effective g factor of a bulk hole from the Γ_8 subband with $J = \frac{3}{2}$ [44,53]:

$$\begin{aligned} g_h &= \frac{E_{-J_{hz}} - E_{+J_{hz}}}{2J_{hz}\mu_B B} \\ &= \frac{E_{-3/2} - E_{+3/2}}{3\mu_B B} = \frac{E_{-1/2} - E_{+1/2}}{\mu_B B}, \end{aligned} \quad (7)$$

where J_{hz} is the hole spin projection on the magnetic field direction. A positive g_h corresponds to the hole ground state with a positive spin projection J_{hz} . It is convenient to write the effective Zeeman Hamiltonian (5) as

$$\hat{H}_Z^{(h)} = -\mu_B g_h J_{hz} B. \quad (8)$$

The Hamiltonian (8) describes the splitting of the otherwise fourfold-degenerate hole ground state in bulk crystals, as well as in spherically symmetric structures. For example, in bulk semiconductors with large Δ_{SO} , the Zeeman effect for both light ($J_{hz} = \pm\frac{1}{2}$) and heavy ($J_{hz} = \pm\frac{3}{2}$) holes is characterized by the same g factor $g_h \equiv g_h^{\text{bulk}} = 2\kappa$. Note that the actual Zeeman splitting of heavy holes is three times larger than that of light holes for the same g factor: $\Delta E_{3/2} = 3\Delta E_{1/2}$. The scheme of hole energy-level splitting both in the electron and hole representations for noninteracting electron and hole is shown in Fig. 1. As we are interested in holes in the Γ_8 subband we do not show here the Γ_7 valence subband. The definition (7) and the Hamiltonian (8), which will be used hereafter, are widely used in the physics of colloidal nanocrystals with J_{hz} being changed by the total angular momentum projection M [22,44,54–57].

Another definition of the hole g factor with the opposite sign as compared with (7) and (8) is also used in the literature (see, for example, Refs. [45,50,58,59]). For structures with a large light- and heavy-hole splitting, the heavy-hole g factor is often defined as $\Delta E_{3/2} = E_{+3/2} - E_{-3/2} = \mu_B g_{hh} B$ with $g_{hh} = -3g_h = -6\kappa$ [45,58] describing the whole Zeeman splitting of heavy holes. While all definitions of the hole g factor follow from the same Zeeman contribution to the hole Hamiltonian (5) and describe the same energy splitting of hole states in the magnetic field, one should carefully consider the chosen definition when comparing of the calculated g factors with experimentally evaluated data.

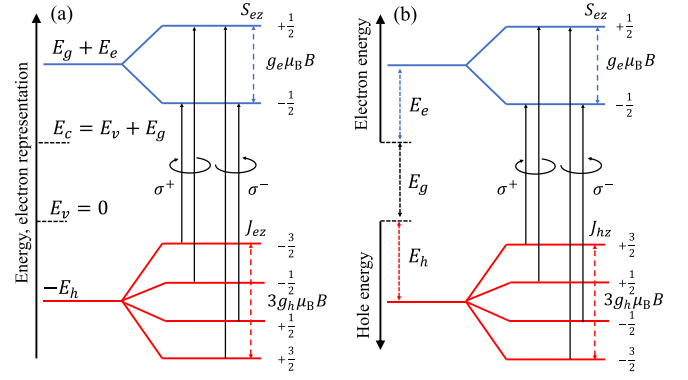


FIG. 1. The scheme of Zeeman energy-level splitting of electrons and Γ_8 holes in bulk zb semiconductor (a) in electron and (b) in mixed electron-hole representations. E_h and E_e are hole and electron energy levels in zero magnetic field calculated from the top of the valence band $E_v = 0$ and the bottom of the conduction band $E_c = E_g$, respectively. The order of electron and hole levels is shown for $g_e > 0$, $g_h > 0$, in the limit $\mu_B B \ll \Delta_{SO}$. The circularly polarized optical transitions are denoted by σ^+ and σ^- .

The orbital contribution from the magnetic field to the hole Hamiltonian \hat{H}_B comes from the hole wave vector \mathbf{k} being replaced by $\mathbf{k} - \frac{e}{c}\mathbf{A}$, with \mathbf{A} being the vector potential of magnetic field. For simplicity, we consider the magnetic field \mathbf{B} directed along the z axis being also one of the crystal axis. As we consider the hole Hamiltonian in spherical approximation, doing so does not lead to the loss of generality of results. The explicit form of \hat{H}_B can be found in Appendix B (in the units of $\mu_B B$), in the limit $\Delta_{SO} \rightarrow \infty$ its part corresponding to Γ_8 holes coincides with the Hamiltonian presented in Ref. [42]. For a bulk hole \hat{H}_B contribution vanishes in weak magnetic field.

In semiconductors with the cubic lattice symmetry, one can also separate the cubically symmetric contribution to the Zeeman part of the hole Hamiltonian, originating from the valence band warping $\propto q(B_x J_x^3 + B_y J_y^3 + B_z J_z^3)$. However, generally parameter q is small, and the cubic contribution to the hole Zeeman splitting is much smaller than the isotropic $\hat{H}_Z^{(h)}$ and \hat{H}_B [60].

B. Renormalization of the hole effective g factor in low-dimensional structures

The last term $V_{\text{ext}}(\mathbf{r})$ in Eq. (3) is a nanostructure potential acting on the hole. The main effect of $V_{\text{ext}}(\mathbf{r})$ on the hole g factor is the mixing of hole states from different subbands. As a result, for localized holes, the internal angular momentum and its projections are not good quantum numbers. In spherically symmetric systems, the states can be classified by the hole total angular momentum [52,61–63]. In axially symmetric structures the total angular momentum projection on the symmetry axis can be used [62,64]. In structures with an inversion center, one can use a state “parity” as a quantum number to classify hole states [64,65]. The states with odd and even parity are an analog of electron spin-up and -down states and are degenerate in zero magnetic field.

The hole states in nanostructure are characterized by the total angular momentum projection M on its symmetry axis,

which coincides with the z direction. With the magnetic field $\mathbf{B} \parallel z$ one can use the definitions similar to Eqs. (7) and (8) for the hole effective g factor and Zeeman term, respectively, with J_{hz} replaced by M . Except for the spherically symmetric structures, the Zeeman splitting of light and heavy subbands might be controlled by different g factors depending on $|M|$, so we define

$$g_{h,|M|} = \frac{E_{-M} - E_{+M}}{2M\mu_B B}, \quad \widehat{H}_Z^{(h)} = -\mu_B g_{h,|M|} M B. \quad (9)$$

The first correction to the hole effective g factor as compared with the bulk case comes from the renormalization of the Zeeman term ($\propto \varkappa$ for holes from the Γ_8 valence band if admixing of spin-split holes is negligible), Eq. (5). This renormalization $\langle \Psi_M | \widehat{J}_{hz} | \Psi_M \rangle / M$ is a function of the mass ratio $\beta = m_{lh}/m_{hh} = (\gamma_1 - 2\gamma)/(\gamma_1 + 2\gamma)$ and Δ_{SO}/E_h and is caused by the mixing of hole states from different subbands with different bulk g factor. The second one is related to the orbital contribution $\propto \gamma_1$, γ and is also controlled by some function of β and Δ_{SO}/E_h . For numerical calculations, we considered zinc zb-CdSe and InP and wurtzite modification of CdSe, where the crystal field energy $\Delta_{cr} \ll \Delta_{SO}$. In relatively small NCs with $\Delta_{cr} \ll E_h$, our numerical calculation has shown that the crystal field effect can be treated as a small perturbation. It results in the splitting of the states with $|M| = \frac{3}{2}$ and $\frac{1}{2}$ in zero magnetic field $\leq \Delta_{cr}$ without modification of the hole wave function. In this case, the effective crystal field perturbation $\propto \Delta_{cr}$ does not affect the hole g factors, while magnetic field is weak enough. Thus, the crystal field and magnetic field perturbations can be taken into account separately, and both the light- and heavy-hole Zeeman splitting in wurtzite NCs can be described by our calculation for zinc-blende NCs with the same set of the valence band parameters.

III. HOLE g FACTOR IN SPHERICAL AND CUBE NANOSTRUCTURES

A. Spherical nanocrystals

A spherically symmetric external potential represents the special case of the highest possible symmetry, in which hole states are classified by their total angular momentum [52,61–63]. Following [66] we write the six-component hole envelope function as

$$\Psi_M = \sqrt{2j+1} \sum_l (-1)^{l-J+M} (i)^l R_{jlJ}(r) \times \sum_{m+\mu=M, J=3/2, 1/2} \begin{pmatrix} l & J & j \\ m & \mu & -M \end{pmatrix} Y_{l,m} u_{J,\mu}. \quad (10)$$

Here $\mathbf{j} = \mathbf{J} + \mathbf{l}$ is the hole total angular momentum with M being its z -axis projection, l is the hole orbital momentum, Y_{lm} are spherical harmonics [67], $\begin{pmatrix} i & k & l \\ m & n & p \end{pmatrix}$ are $3j$ Wigner symbols, and u_μ are the Bloch functions of the Γ_8 and Γ_7 top valence subbands with spin z -axis projection μ [49,68] [for details see Appendix B, Eq. (B1)]. We will study the g factor of the fourfold-degenerate hole state with $j = \frac{3}{2}$ which consists of functions with $l = 0$ and $l = 2$ (SD -like state). In the limit $\Delta_{SO} \rightarrow \infty$ it is the ground state of the hole both in the boxlike and parabolic potentials [69]. We denote the respective radial functions as $R_{3/2,0,3/2} \equiv R_0$, $R_{3/2,2,3/2} \equiv R_2$, $R_{3/2,2,1/2} \equiv R_s$.

Taking into account the spherical symmetry of the structure, one can simplify the Schrödinger equation to the system of three equations for R_0 , R_2 , and R_s [66,70], which reduces to the system of two equations for R_0 and R_2 in the limit $\Delta_{SO} \rightarrow \infty$ [52]. For the boxlike infinite potential radial wave functions R_0 , R_2 and R_s have analytical form (see Ref. [70]) (the limit $\Delta_{SO} \rightarrow \infty$ was studied in Refs. [71,72]). For the parabolic potential, calculations were made numerically using the generalized for the six-band Hamiltonian numerical method introduced in Refs. [42,43]. While the energy of the SD -like state in zero magnetic field E_0 depends on β , its dependence on the NC radius a is controlled by the characteristic heavy-hole quantization energy $E_h = \hbar^2 \pi^2 / 2m_{hh} a^2$ for the boxlike potential and $E_h = 3\hbar^2 / 2m_{hh} L_h^2$ for the parabolic potential with L_h being the heavy-hole oscillator length. Note that E_h corresponds to the hole quantum size quantization energy in the respective potential in the case $\beta = 1$ (the limit of the simple valence band), while the level energies increase with decrease of $\beta < 1$ in both potentials [43].

In the external magnetic field the fourfold-degenerate ground state splits into four equidistant levels with $M = \pm \frac{3}{2}, \pm \frac{1}{2}$. As in the bulk case, such a splitting is characterized by a single g factor $g_{h,3/2} = g_{h,1/2} = g_h \equiv g_h^{\text{sph}}$ according to Eq. (9). The expression for $g_h \equiv g_h^{\text{sph}}$ in the four-band Luttinger model was first obtained in Ref. [53] for the hole bound to the acceptor Coulomb potential. We generalize it for the six-band model as

$$g_h^{\text{sph}} = 2\varkappa + \frac{4}{5}I_1^g + \frac{4}{5}I_2^g(\gamma_1 - 2\gamma - 2\varkappa) + \frac{2}{5}I_3^g(-1 - 3\gamma_1 - 7\varkappa) - \frac{2}{5}\gamma I_4^g - \frac{8}{5}I_5^g(1 + \varkappa), \quad (11)$$

$$I_1^g = \frac{1}{2} \int r^3 dr \left(R_2 \frac{dR_0}{dr} - R_0 \frac{dR_2}{dr} - \frac{3}{r} R_0 R_2 \right),$$

$$I_2^g = \int r^2 dr R_2^2, \quad I_3^g = \int r^2 dr R_s^2,$$

$$I_4^g = \int r^3 dr \left((R_2 + 3R_0) \frac{dR_s}{dr} + \frac{9}{r} R_s (R_0 - R_2) \right)$$

$$- \int r^3 dr \left(3R_s \frac{dR_0}{dr} + R_s \frac{dR_2}{dr} \right), \quad I_5^g = \int r^2 dr R_2 R_s.$$

Integrals I_{1-5}^g , for a given potential profile and fixed ratio between the hole quantization energy E_h and Δ_{SO} depend only on the light- to heavy-hole effective mass ratio β . Integrals I_1^g and I_2^g were first derived within the four-band Luttinger model [53]. If the hole wave function vanishes at the NC surface, one can simplify the expression for the I_1^g [53] and I_4^g by partial integration. To separate the renormalization of the Zeeman and orbital contributions to the hole g factor we rewrite Eq. (11) as

$$g_h^{\text{sph}} = 2[\varkappa S(\beta) - S_c(\beta)] + \gamma_1 I(\beta), \quad (12)$$

where

$$S(\beta) = 1 - \frac{4}{5}I_2^g - \frac{7}{5}I_3^g - \frac{4}{5}I_3^g, \quad S_c(\beta) = \frac{1}{5}(I_3^g + 4I_5^g),$$

$$I(\beta) = \frac{(1-\beta)}{5(1+\beta)}(4I_1^g - I_4^g + 6I_3^g) + \frac{4\beta}{5(1+\beta)}(2I_2^g + 3I_5^g).$$

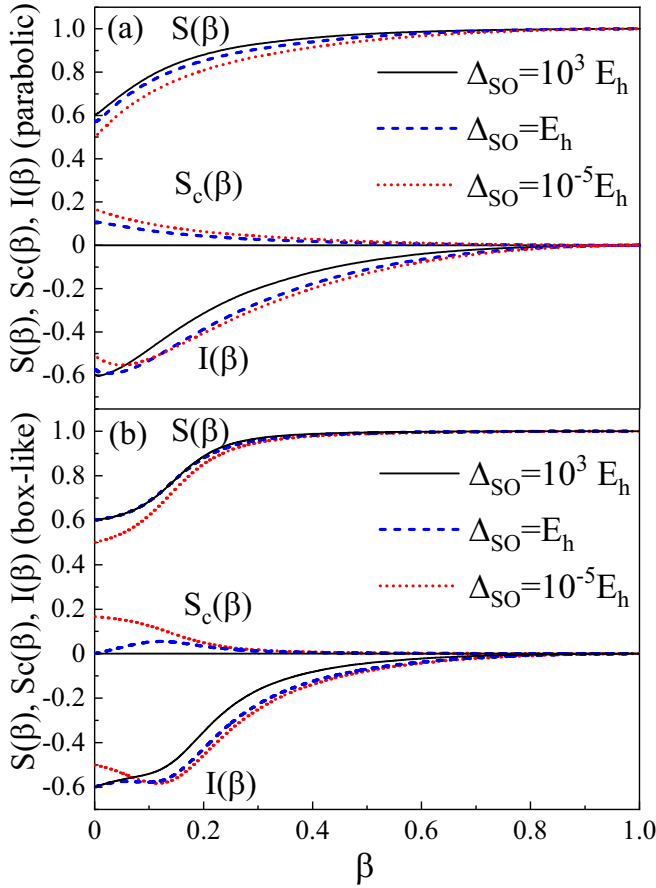


FIG. 2. Functions $S(\beta)$, $S_c(\beta)$, and $I(\beta)$ in NCs with (a) parabolic and (b) abrupt boxlike potential, calculated for Δ_{SO} much larger (solid black curves), much smaller (dotted red curves), and comparable (dashed blue curves) with heavy-hole characteristic energy E_h defined in the text.

Functions $S(\beta)$ and $S_c(\beta)$ describe the renormalization of the Zeeman contribution \hat{H}_Z^h and function $I(\beta)$ describes the orbital contribution to the g factor stemming from \hat{H}_B . In the limit $\Delta_{SO}/E_h \rightarrow \infty$ the radial function R_s vanishes as well as quantities it is contained in, I_{3-5}^s and function $S_c(\beta)$. The hole g factor in this case is expressed by classical formula from Ref. [53]. In the opposite limit of a weak spin-orbit coupling $\Delta_{SO}/E_h \rightarrow 0$, it can be shown that $R_2 \equiv R_s$ and $I_2^s \equiv I_3^s \equiv I_5^s$.

In Fig. 2 we show the dependencies of functions $S(\beta)$, $S_c(\beta)$, and $I(\beta)$ for the parabolic [Fig. 2(a)] and boxlike infinite [Fig. 2(b)] potentials, calculated for Δ_{SO} much larger, much smaller and comparable with the heavy-hole ground-state size quantization energy E_h . In the limit $\Delta_{SO} \gg E_h$, which corresponds to NCs of large radius, the admixture of Γ_7 holes is negligible and presented curves can be calculated using the four-band Luttinger Hamiltonian. $S(\beta)$ and $S_c(\beta)$ are always positive, while $I(\beta)$ is negative. The resulting sign of the hole g factor depends on the interplay of all contributions, tending to be negative in semiconductors with relatively large γ_1 .

B. Cube nanocrystals

Here we consider NCs with an infinite potential of cubic shape or cube NCs with an edge length L (see details in

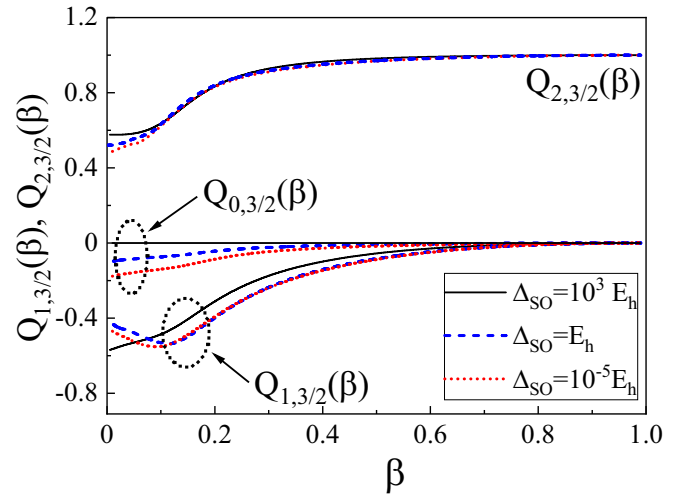


FIG. 3. The dependencies $Q_{1,3/2}(\beta)$ and $Q_{2,3/2}(\beta)$ for the quantum state E_0 in cube NCs for Δ_{SO} much larger (solid black curves), much smaller (dotted red curves), and comparable (dashed blue curves) with the heavy-hole quantization energy $E_h = 3\hbar^2\pi^2/m_{hh}L^2$.

Appendix C), still neglecting the effects of cubic symmetry of the crystal structure. In this case, the system under study loses its spherical and axial symmetry. The total angular momentum and its projection on the magnetic field direction (unless the magnetic field is directed along one of the cubic axes) are not good quantum numbers. In zero magnetic field, the two lowest hole states originating from the Γ_8 subband remain fourfold degenerate since cubic anisotropy does not split states with a total angular momentum less than $\frac{5}{2}$ (as it would be in spherically symmetric NC) [73]. Depending on β , the hole ground state in cube NCs might be a *PF*-like (with energy E_1) state instead of a *SD*-like (with energy E_0) state even in the $\Delta_{SO}/E_h \rightarrow \infty$ limit [see Fig. 12(a)]. In the following, we will focus only on the *SD*-like state.

The hole effective g factors for the light- ($|M| = \frac{1}{2}$) and heavy- ($|M| = \frac{3}{2}$) hole states can be written as

$$g_{h,|M|} = 2[\alpha Q_{2,|M|}(\beta) + Q_{0,|M|}(\beta)] + \gamma_1 Q_{1,|M|}(\beta). \quad (13)$$

Function $Q_{1,|M|}(\beta)$ describes the orbital contribution to the hole g factor and $Q_{2,|M|}(\beta)$ and $Q_{0,|M|}(\beta)$ describe the renormalization of the spin contribution. In contrast to the spherical case, these functions are different for heavy and light holes. The dependencies $Q_{0,|M|}(\beta)$, $Q_{1,3/2}(\beta)$, and $Q_{2,3/2}(\beta)$ for the quantum state E_0 calculated numerically for Δ_{SO} much larger, much smaller, and comparable to the heavy-hole characteristic energy $E_h = 3\hbar^2\pi^2/m_{hh}L^2$, corresponding to the hole size quantization energy for $\beta = 1$, are shown in Fig. 3.

In contrast with spherical NCs, while the *SD*-like hole state in cube NCs is fourfold degenerate in zero field, the g factors of heavy and light holes are different and can have opposite signs. This effect is a manifestation of the breaking of spherical symmetry and can be qualitatively described by the cubic contribution $Q(B_x J_x^3 + B_y J_y^3 + B_z J_z^3)$ to the spherically symmetric hole Hamiltonian with large Q (unlike neglected term with a small q , originating from the cubic symmetry of the crystal lattice). As for spherical NCs, the admixture of Γ_7 holes and the related difference between the six- and

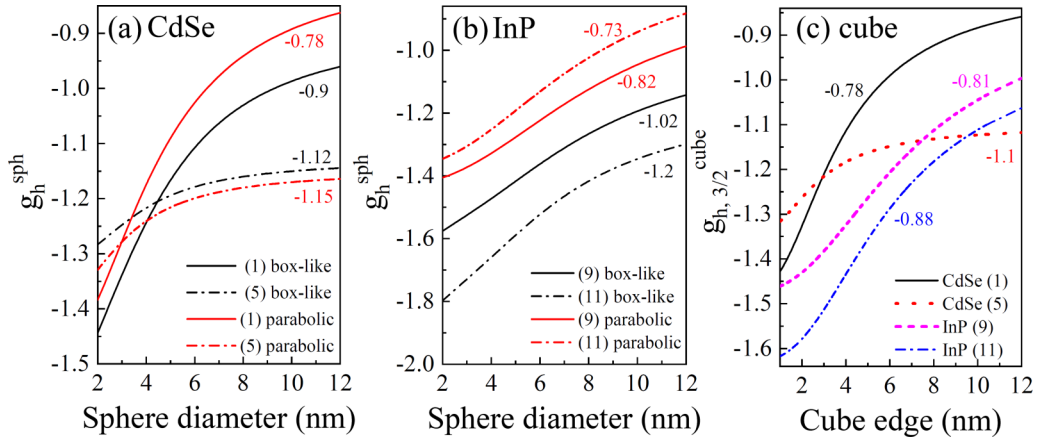


FIG. 4. Hole $1S_{3/2}$ state g_h^{sph} in (a) CdSe (zinc blende and wurtzite) and (b) InP-based spherical NCs as a function of NC diameter for different parametrizations from Table I. In (c) the hole ground-state $g_{h,3/2}^{\text{cube}}$ dependence on the cube edge length in cube nanocrystals is presented. The values of Δ_{SO} are $\Delta_{\text{SO}} = 420$ meV for CdSe and $\Delta_{\text{SO}} = 100$ meV for InP, respectively. The numbers in brackets correspond to the parametrization in Table I, the numbers given near the curves represent the value of the hole g factor calculated within the four-band model.

four-band models are more important for smaller β , including values relevant for real semiconductors.

The size dependencies of the hole g factor for spherical and cube CdSe and InP NCs are shown in Fig. 4. For the sake of comparison, we define the diameter $d = 2a$ of a NC with the parabolic potential as $d = 4L_h$. For both types of confining potential the hole g factor decreases towards small NCs, while for the boxlike potential, the absolute value is larger and the relative change of the g factor is larger for sets of Luttinger parameters corresponding to a smaller effective mass of a heavy hole, i.e., larger quantization energy. One of the main points of Fig. 4 is a strong dependence of calculated value of the hole g factor on the chosen set of valence band parameters, which are listed in Fig. 4. The size dependencies of the hole g factor in Fig. 4 also demonstrate the importance of taking

into account of the Γ_7 band admixture in spherical and cube NCs with the sizes up to 12 nm. We remind that with the increase of NC size and the consequent decrease of the hole size quantization energy, the admixture of the Γ_7 spin-split holes become negligible and the results of the six-band model tend to the results of the four-band model. The corresponding limiting values of the hole g factor are given near the curves, while the bulk g factor values g_h^{bulk} are given in Table I.

C. Spheroidal and cuboid nanocrystals

Here we briefly consider the uniaxial shape distortion of spherical and cube NCs. We assume that the symmetry axis is directed along z . Such an axially symmetric perturbation splits the hole ground state with the total angular momentum $j = \frac{3}{2}$ into two Kramers doublets with momentum projections $M \pm \frac{3}{2}$ and $M \pm \frac{1}{2}$ on the crystal axis, similarly to the effect of the internal crystal field in wurtzite semiconductors. The anisotropy-induced splitting for hole states described by the four-band Luttinger Hamiltonian in NCs with the boxlike infinite potential and the smooth parabolic and Gaussian potentials was studied in Refs. [43,54,72,83]. For the vast majority of Luttinger parameter sets in oblate NCs the ground state has the angular momentum projection $M = \pm \frac{3}{2}$ on NC axis (it will be referred as heavy holes as it consists mostly of Bloch states with $J = \frac{3}{2}$ and $J_{hz} = \pm \frac{3}{2}$), and $M \pm \frac{1}{2}$ (light holes) in prolate NCs [42,43,72]. Below we generalize the calculation of the effect of such NC anisotropy on the heavy- and light-hole g factors $g_{h,3/2}$ and $g_{h,1/2}$ for the six-band hole Hamiltonian (4).

For NCs with the parabolic confining potential

$$V_{\text{ext}}(\mathbf{r}) \equiv V_p^{\text{an}}(\rho, z) = \frac{\kappa_\rho}{2} \rho^2 + \frac{\kappa_z}{2} z^2,$$

where κ_z (κ_ρ) is the potential stiffness along (perpendicular) z axis, we introduce parameter of the shape anisotropy of NC μ as anisotropy of its potential [43]:

$$\mu = \frac{3}{2} \frac{(\kappa_\rho - \kappa_z)}{(2\kappa_\rho + \kappa_z)}.$$

TABLE I. Parametrizations of the valence band parameters.

No.	Material	γ_1	γ	\varkappa	$g_h^{\text{bulk}} = 2\varkappa$	β	Refs. ^a
1	zb-CdSe	5.51	1.78	0.46	0.93	0.22	[74]
2	zb-CdSe	3.27	1.33	0.46	0.93	0.1	[75]
3	zb-CdSe	3.8	1.65	0.81	1.62	0.07	[75]
4	zb-CdSe	2.52	0.83	-0.12	-0.25	0.2	[76]
5	wz-CdSe	2.04	0.58	-0.38	-0.76	0.28	[77]
6	wz-CdSe	1.7	0.4	-0.57	-1.13 ^b	0.36	[78]
7	wz-CdSe	2.1	0.55	-0.45	-0.9	0.31	[66]
8	wz-CdSe	1.67	0.56	-0.29	-0.58	0.2	[79]
9	InP	5.05 ^c	1.68 ^c	0.45	0.9	0.2	[80]
10	InP	4.6 ^c	1.68 ^c	0.6	1.2	0.15	[80]
11	InP	5.25	1.9	0.75	1.5 ^b	0.16	[81]
12	InP	4.94	1.79	0.67	1.34	0.16	[76]

^aReferences are given for the γ_1 , γ_2 , and γ_3 Luttinger parameters. We use relations $\gamma = (2\gamma_2 + 3\gamma_3)/5$ [82] and $\varkappa \approx -2/3 + 5\gamma/3 - \gamma_1/3$ [31].

^bExperimental g factors of a bulk hole determined by Landau level spectroscopy.

^cExperimental values from the hot photoluminescence measurements.

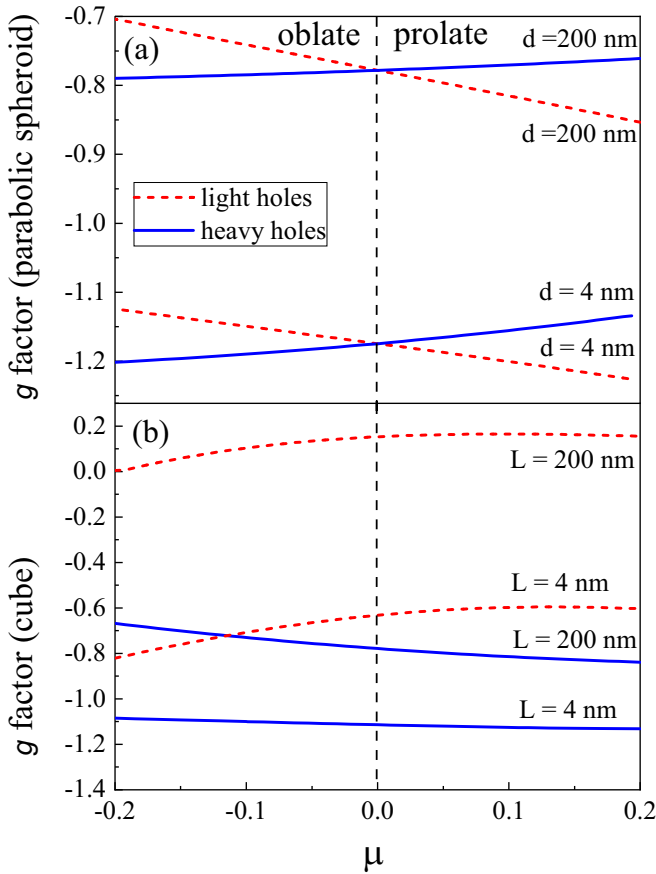


FIG. 5. The dependencies of the light-hole $g_{h,1/2}$ and heavy-hole $g_{h,3/2}$ g factors on the anisotropy parameter μ in (a) spheroidal NCs with the parabolic potential with $d = 200$ nm and $d = 4$ nm and (b) cuboid NCs with the boxlike infinite potential with edge length $L = 200$ nm and 4 nm. The calculations are done for zb-CdSe parameters given by parametrization 1 in Table I and $\Delta_{SO} = 420$ meV.

For spheroidal NCs with the infinite boxlike potential at the surface and shape described by $x^2/b^2 + y^2/b^2 + z^2/c^2 = 1$, the small shape anisotropy parameter μ is introduced by $\mu = c/b - 1$ with $c \approx a(1 - 2\mu/3)$, $b \approx a(1 + \mu/3)$. The zero-order approximation corresponds to a sphere of the radius a . The first-order perturbation is obtained after the coordinate change to $x \rightarrow xa/b$, $y \rightarrow ya/b$, $z \rightarrow za/c$ [72]. Similarly, this method can be applied to treat the anisotropy of NCs of square cuboid shape with the infinite boxlike potential and dimensions $2b$ and $2c$, and zero-order approximation being the cube with the edge $L = 2a$.

In Fig. 5 the heavy- and light-hole g factors $g_{h,3/2}$ and $g_{h,1/2}$ as functions of μ are shown. Calculations were made for the zb-CdSe parameters set 1 (Table I) and $\Delta_{SO} = 420$ meV, for spheroidal/cuboid NCs with the diameter/edge 200 nm, where the admixture of Γ_7 holes is negligible so that the same result can be obtained within the four-band model, and 4 nm (the admixture is important). For both sizes curves look very similar, although the values of the g factors are quite different.

From Fig. 5(a) one can see that in spheroidal NCs the light- and heavy-hole g factors are different. This demonstrates that, while the shape anisotropy results in the splitting of the states with $|M| = \frac{3}{2}$ and $\frac{1}{2}$ similar to the effect of the crystal field

in wurtzite NCs, one can not treat magnetic field and shape anisotropy perturbations separately. As our analysis showed, the corrections to the heavy- and light-hole g factors coming from the NC shape anisotropy can be calculated by the perturbation theory as the first-order corrections coming from the \hat{H}_B , using wave functions, already taking into account the shape anisotropy in zero magnetic field. As a consequence, like in cube NCs, in “quasispherical” wurtzite NCs where the light- and heavy-hole splitting caused by the shape anisotropy compensates the crystal field splitting [18] and the hole state is fourfold degenerate in zero magnetic field, the case $g_{h,3/2} \neq g_{h,1/2}$ is realized.

IV. HOLE g FACTOR IN 2D NANOCRYSTALS

A. Quantum well of infinite lateral size

In quantum-well-like NCs, i.e., nanoplatelets (NPLs), where the thickness L is much smaller than the in-plane dimensions, the heavy- and light-hole states are strongly split in zero magnetic field. In quantum-well-like NCs, i.e., nanoplatelets (NPLs), where the thickness L is much smaller than the in-plane dimensions, the heavy- and light-hole states are strongly split in zero magnetic field. For example, the reported values for such splitting in 4 monolayers (ML) CdSe NPL are about 180 meV [84] and about 150 meV [85]. In the in-plane isotropic NPL, the hole ground state is characterized by the total angular momentum projection $M = \pm \frac{3}{2}$ on the symmetry axis directed perpendicular to the NPL plane (z axis) is composed only of the heavy-hole valence band states with $J = \frac{3}{2}$ and $J_{hz} = \pm \frac{3}{2}$ with a vanishing admixture of light and spin-split holes. Therefore, in the limit of a two-dimensional (2D) structure with the vanishing width to in-plane size ratio there is no renormalization of the spin Zeeman effect. However, as it is was shown in Ref. [86], the orbital contributions to the heavy-hole g factor $g_{h,3/2}^{2D} \equiv g_{h,3/2}^{2D}$ coming from the \hat{H}_B in the first-order perturbation theory for a magnetic field directed along the symmetry axis are present due to the quantization of k_z and the magnetic field-induced heavy- and light-hole mixing. We modified the expression from Ref. [86] to take into account the admixture of holes from the Γ_7 valence subband. In NPLs, as in all other quantum-well-like structures, light holes are mixed effectively with spin-split holes if Δ_{SO} is comparable or smaller than the heavy-hole size quantization energy $E_h = \hbar^2 \pi^2 / 2m_{hh}L^2$ for the boxlike potential and $E_h = \hbar^2 / 2m_{hh}L_h^2$ for the parabolic potential. So, to use the perturbation theory one has to construct a proper zeroth-order approximation function and the proper perturbation Hamiltonian (see Appendix B). After doing so, we arrive to the expression

$$g_{h,3/2}^{2D} = 2\chi - 4 \frac{\hbar^2}{m_0} \sum_{n=1}^{\infty} \frac{|\langle \tilde{I}h_{2n} | \gamma \hat{k}_z | hh_1 \rangle|^2}{\tilde{E}_{Ih_{2n}} - E_{hh_1}} A_1 \left(\frac{\Delta_{SO}}{E_{hh_1}}, \beta \right)^2 - 2 \frac{\hbar^2}{m_0} \sum_{n=1}^{\infty} \frac{|\langle \tilde{S}O_{2n} | \gamma \hat{k}_z | hh_1 \rangle|^2}{\tilde{E}_{SO_{2n}} - E_{hh_1}} A_2 \left(\frac{\Delta_{SO}}{E_{hh_1}}, \beta \right)^2. \quad (14)$$

Here $|hh_1\rangle$ is the envelope wave function of the heavy-hole ground state of the quantization along the z axis, $|\tilde{I}h_{2n}\rangle$ and $|\tilde{S}O_{2n}\rangle$ are new wave functions of even excited states of the light hole and spin-split hole $E_{hh_1} \equiv E_h$, $\tilde{E}_{Ih_{2n}}$ and $\tilde{E}_{SO_{2n}}$ are

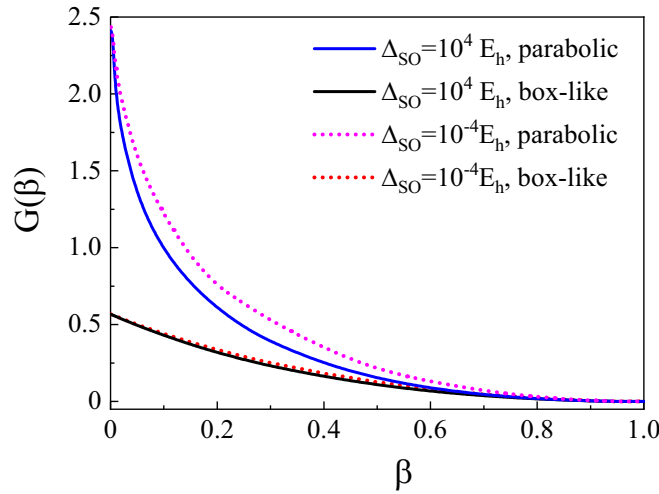


FIG. 6. Function $G(\beta)$ calculated for the parabolic and boxlike infinite potentials in two limiting cases: Δ_{SO} much larger (solid curves) and much smaller (dotted curves) than the heavy-hole quantization energy E_h defined in the text.

the corresponding energies. Coefficients $A_1(\frac{\Delta_{\text{SO}}}{E_{hh1}})$ and $A_2(\frac{\Delta_{\text{SO}}}{E_{hh1}})$ describe the magnetic-field-induced perturbation to the heavy hole in new basis. In general case energies $\tilde{E}_{lh_{2n}}$ and $\tilde{E}_{SO_{2n}}$, wave functions $\tilde{l}h_{2n}$ and $\tilde{S}O_{2n}$, and coefficients $A_1(\frac{\Delta_{\text{SO}}}{E_{hh1}})$ and $A_2(\frac{\Delta_{\text{SO}}}{E_{hh1}})$ can not be calculated analytically. The expressions for structures with the boxlike potential are presented in Appendix B. In the limit $\Delta_{\text{SO}} \rightarrow \infty$ we have $A_1(\frac{\Delta_{\text{SO}}}{E_{hh1}}, \beta) \rightarrow -1$, $A_2(\frac{\Delta_{\text{SO}}}{E_{hh1}}, \beta) \rightarrow -1/\sqrt{2}$, $\tilde{E}_{SO_{2n}} \rightarrow \infty$ and Eq. (14) tends to a well-known formula [86]

$$g_{h,3/2}^{2D} = 2\kappa - 4 \frac{\hbar^2}{m_0} \sum_{n=1}^{\infty} \frac{|(lh_{2n}|\gamma\hat{k}_z|hh_1)|^2}{E_{lh_{2n}} - E_{hh1}}. \quad (15)$$

Here $|hh_1\rangle$ is the envelope wave function of the heavy-hole ground state of the quantization along the z axis, $|lh_{2n}\rangle$ are wave functions of even excited states of the light hole, and $E_{lh_{2n}}$ are the corresponding energies.

After summation Eq. (14) can be written as

$$g_{h,3/2}^{2D} = 2\kappa - \frac{\gamma_1}{3} G(\beta), \quad (16)$$

where $G(\beta)$, with fixed Δ_{SO} depends only on β and the type of the localization potential along the z direction.

The dependencies of $G(\beta)$ on β for the parabolic and boxlike infinite potentials are shown in Fig. 6 for large (solid curves) and small (dotted curves) Δ_{SO} . The dependence for parabolic potential is stronger due to smaller distances between hole energy levels as compared with the boxlike potential. Note that unlike spherical and cube NCs, for NPLs the dependence of $G(\beta)$ and, consequently, hole g factor on the ratio Δ_{SO}/E_h is much weaker. In most cases one can use results obtained within the four-band model in the limit $\Delta_{\text{SO}} \rightarrow \infty$ for estimation of the heavy-hole g factor, especially for the boxlike potential. Note that despite the relatively weak dependence of the hole g factor on the NPL thickness for NPLs with infinite lateral size, especially for the boxlike potential, the mixing of the light holes and spin-split-off holes in thin NPLs is strong [87,88].

B. Nanoplatelet with a finite in-plane size

Realistic colloidal NPLs have finite thickness and finite in-plane size [85,89,90]. This makes the situation different from the one in epitaxial thin quantum well. The finiteness of the ratio of the NPL thickness to the in-plane size results in nonzero light- and heavy-hole mixing even in zero magnetic field. This leads to a nonzero first-order perturbation renormalization of the spin Zeeman term, as well as to orbital correction to the hole effective g factor. As a consequence, the hole ground-state g factor is somewhere in-between the 2D, $g_{h,3/2}^{2D}$, and spherical, g_h^{sph} , limits. In Fig. 7 we show the dependencies of the hole ground-state g factor on the NC width L for different in-plane cross sections $L_x \times L_y$ for the [Figs. 7(a) and 7(c)] parabolic and [Figs 7(b) and 7(d)] boxlike infinite potentials. For NCs with the parabolic potential, we define the L_α along each direction $\alpha = x, y, z$ as $L_\alpha = 4L_{h,\alpha}$, where $L_{h,\alpha}$ is the oscillator length along respective direction calculated with the heavy-hole effective mass. The calculations are done for the zb-CdSe parameters given in Table I, parametrization 1, using the six-band Hamiltonian (4) for holes.

One can see from Fig. 7 that in the limit $L = L_z \rightarrow 0$ for both potentials asymptotic values for each in-plane size are different due to size dependence of the hole g factor coming from the six-band Hamiltonian (mixing light and spin-split holes). Dashed lines in both panels correspond to the value of the heavy-hole g factors in cube (spherical) NC of zb-CdSe with in-plane size $8 \times 8 \text{ nm}^2$: $g_h^{\text{sph}} \approx -0.81$ and $g_{h,3/2}^{\text{cube}} \approx -0.92$.

In Fig. 7 we also show the dependence of the heavy-hole g factor in NPL with infinite in-plane size (2D limit). For the limiting curves one can see a weaker size dependence, especially for NPLs with the boxlike infinite potential. For conventional quantum wells one can safely neglect the admixture of Γ_7 holes for both types of localizing potential, and for NPLs with smaller width for the boxlike potential.

Dependence of the $g_{h,3/2}$ on the NPL in-plane size comes from the Zeeman contribution as well as from orbital due to mixing of heavy holes with light and Γ_7 holes by the NPL potential. Overall, the smaller the in-plane cross section is, $L_x \times L_y$, the stronger is the g -factor dependence. For cross section $8 \times 8 \text{ nm}^2$ at $L_z = 8 \text{ nm}$ the case of spherical (cube) NCs is realized, and at $L_z > 8 \text{ nm}$ the case of prolate NC with the ground state being the light hole is realized. It leads to the discontinuity of the ground-state g factor in boxlike NCs and to the knee in the g -factor dependence for parabolic NCs. Note that for realistic CdSe NPLs thickness of 1.1 nm (3 ML)–2.3 nm (7 ML), the variation of the hole g factor is mostly driven by NPL lateral size [see Figs. 7(a) and 7(b)]. It opens the possibility of adjusting the hole g factor between sphere/cube and 2D limit by varying the NPL lateral dimensions. Note that the eight-band model, which accounts for the admixture of states from conduction band, may lead to additional height dependence of the heavy-hole g factor, especially for narrow-band-gap semiconductors such as InAs [48].

V. DISCUSSION

In this section, we compare our results with published theoretical and experimental data. Above we have demonstrated

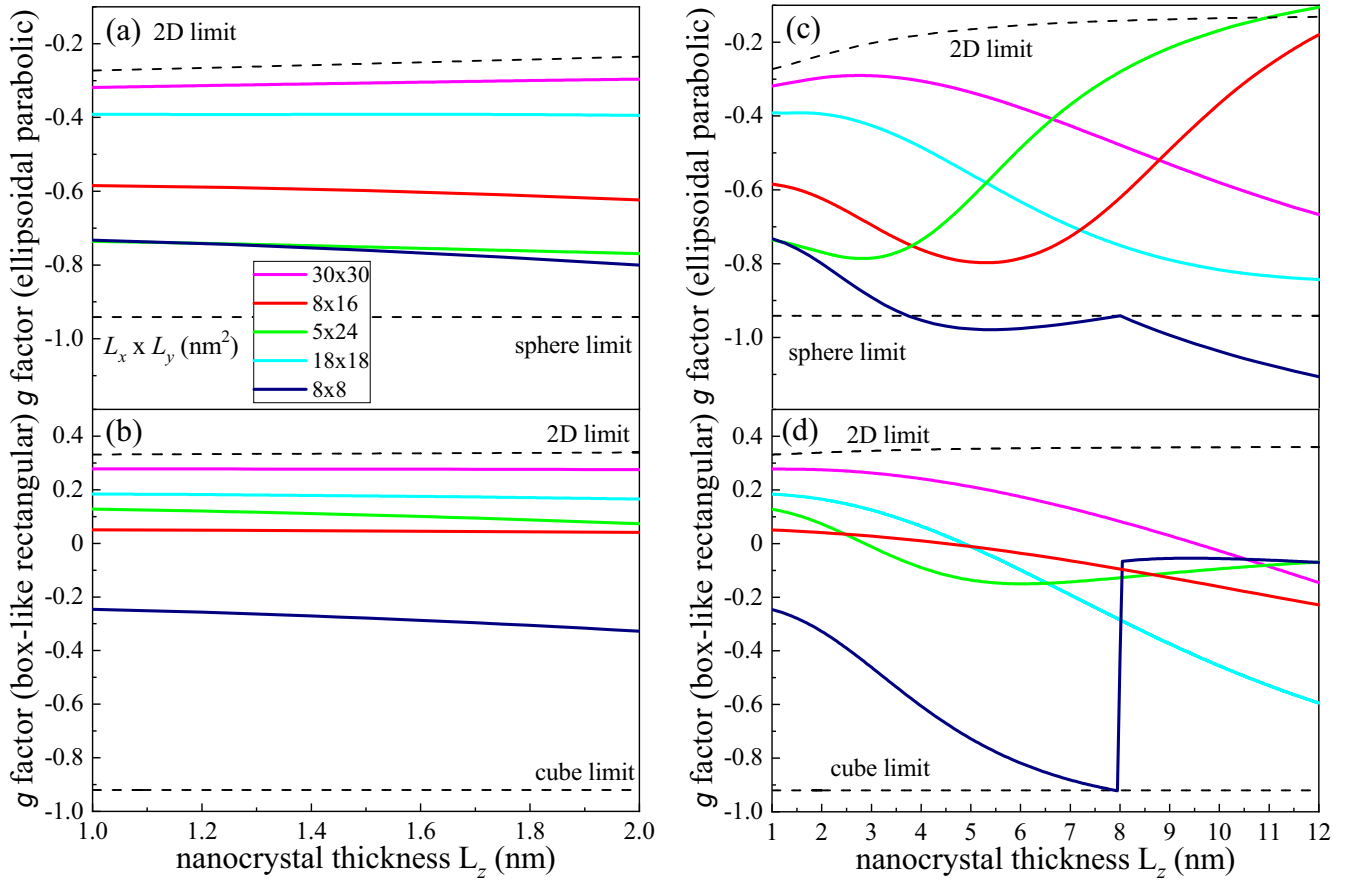


FIG. 7. The dependence of the heavy-hole g factor on NPL width L_z for structures with the (a), (c) parabolic and (b), (d) boxlike infinite potential, calculated for zb-CdSe, parametrization (1) from Table I. The curves of different colors correspond to different NPL in-plane sizes shown as $L_x \times L_y$ in nm^2 . The dashed horizontal lines correspond to the g -factor value in (a), (c) spherical and (b), (d) cube CdSe NCs with diameter (size) 8 nm: $g_h^{\text{sph}} \approx -0.94$ and $g_{h,3/2}^{\text{cube}} \approx -0.92$.

that the admixture of the Γ_7 valence subband results in size dependence of the hole g factor in NCs of different shape. The admixture effect becomes crucial in small NCs, where the hole quantization energy is comparable with the spin-orbit splitting of the valence band. Interestingly, the heavy-hole g factor in thin NPLs with large lateral size (analog of a quantum well) is relatively weak. The largest contribution to the hole g -factor size dependence in NPLs comes from the variation of the lateral size.

In our model, we have neglected the additional renormalization of the valence band Luttinger parameters γ_1 , γ , and \varkappa caused by the quantum confinement of holes, which is similar to the effect of the nonparabolic energy dispersion for electrons [91]. This effect can be taken into account within the eight-band Kane model [45,48,92] and results in additional size dependence of the hole g factor [25,38,45,48]. This effect might be important for extremely small NCs and thin NPLs as well as in narrow-band semiconductors if the hole size quantization energy E_h is comparable with E_g , although it is expected to be smaller than the effect of the admixture of Γ_7 holes as usually $E_g \gg \Delta_{\text{SO}}$. In Ref. [30] the results of tight-binding calculation of the hole g factors in CdSe NCs are presented, demonstrating a strong variation of hole g factor with NC size for a given NC shape, although a direct comparison with our results is difficult.

In the analysis presented above, the quadratics on the magnetic field terms were neglected. Their account results in the magnetic field dependence of the hole g factor in the strong-field regime due to additional hole states mixing if the Zeeman splitting becomes comparable with the hole size quantization energy [46,64,93]. Experimentally, the described effect was observed in quantum wells (e.g., [46,94,95]). In our work we considered the spin-orbit interaction in the valence band independent of the hole wave vector \mathbf{k} . There are also linear on \mathbf{k} contributions in wurtzite semiconductors [96] or in structures with the inversion asymmetry. These terms lead to an additional spin-orbital contribution to the hole g factor as it was demonstrated in Ref. [97] for bulk wurtzite semiconductors. An account of such spin-orbit coupling effects neglected in our calculations would somewhat modify our results, probably improving the agreement between the theory and experiment.

Analyzing experimental data, one has to pay attention to how the hole g factor is defined [we use definitions (7) and (9)] and how it is measured in a particular experiment. One can directly measure the electron g factor in NCs using the spin-flip Raman scattering [98] or pump-probe Faraday rotation technique [18,99–101]. The comparison of the experimental results and theoretical calculations is discussed in Appendix A. Unfortunately, no direct experimental access to the hole g

factor in semiconductor NCs was reported up to now. However, one can use indirect methods to determine the hole g factor from analysis of other measurable parameters.

For example, the hole g factor can be extracted from the magnetic field dependence of the degree of circular polarization (DCP) of the photoluminescence (PL) of negatively charged excitons (negative trions). The PL polarization induced by the external magnetic field is controlled by the difference in populations of the hole Zeeman sublevels in the trion initial state as electron spins are in the singlet state. As a result, the equilibrium polarization is determined by the hole g factor solely.

According to this method for spherical CdSe/CdS NCs with zinc-blende core of 2.5 nm diameter and wurtzite shell of the 10-nm thickness $g_h = -0.54$ was determined [22], which is smaller than the values calculated in the frameworks of both the four- and six-band models. It probably points to the leakage of the hole wave function into the CdS shell.

For CdSe/CdS NPLs with 1.2-nm-thick CdSe core and 8.4-nm-thick CdS shell and about 30-nm side lengths [102] $g_h = -0.4$ was reported (changing to $g_h = -0.7$ in strong magnetic field), which is close to those calculated by us for the parabolic potential [see the curve for the $30 \times 30 \text{ nm}^2$ NPL in Figs. 7(a) and 7(c)], especially if one assumes larger effective width of the NPL caused by the hole leakage to the shell. For bare-core CdSe NPLs with 4- and 5-ML thickness and in-plane sizes 5×24 and $8 \times 16 \text{ nm}^2$ value $g_h \approx -0.1$ (in the range of -0.03 and -0.2) was reported [55,56] which is relatively close to calculated values in the boxlike potential [see Figs. 7(b) and 7(d)]. In both cases we deal with trions formed by heavy hole so that $g_h \equiv g_{h,3/2}$.

While the DCP of the negative trion emission is controlled by the hole g factor, the energies of the respective optical transitions are determined by Zeeman splittings of initial and final states. In this case, both the hole and electron g factor play a role. The equal energies $E_{\sigma^+}^{hh}$ and $E_{\sigma^-}^{hh}$ of four transitions allowed in σ^+ and σ^- polarization and involving the heavy and light holes correspond to the interband transitions are shown schematically in Fig. 1:

$$\begin{aligned} E_{\sigma^+}^{hh} &= \mp \frac{1}{2} g_e \mu_B B \mp \frac{3}{2} g_{h,3/2} \mu_B B \equiv \pm \frac{1}{2} g_1^{hh} \mu_B B, \\ E_{\sigma^-}^{hh} &= \pm \frac{1}{2} g_e \mu_B B \mp \frac{1}{2} g_{h,1/2} \mu_B B \equiv \pm \frac{1}{2} g_1^{lh} \mu_B B. \end{aligned} \quad (17)$$

Equation (17) remains valid in the presence of the uniaxial splitting $\Delta \ll \Delta_{SO}$ of light and heavy holes and the external magnetic field directed along the z direction. In Ref. [21], the analysis of four transition peaks evolution with the magnetic field in the unpolarized PL spectra of singly charged zb-CdSe/CdS/ZnS core/shell/shell NCs with 5.4-nm core diameter allowed to estimate the electron and hole g factors. For spherical NCs, $|g_h| \approx 0.75$ was determined.

For neutral excitons the analysis of magneto-optical data is complicated by the exciton fine-energy structure in zero magnetic field, which varies strongly with the shape and size of NCs. The exchange interaction mixes the exciton states formed with heavy and light holes into the states with the total spin $\mathcal{F} = 1$ and $\mathcal{F} = 2$ split by Δ_{exch} in the case of $\Delta = 0$. The joint action of the exchange interaction and anisotropic splitting leads to the formation of five exciton states in zero magnetic field labeled by the total spin projection $F \equiv \mathcal{F}_z$ on

the anisotropic axis as shown in Fig. 8 for the limits $\Delta \gg \Delta_{exch}$ (a), $\Delta = 0$ (b), and $\Delta \ll \Delta_{exch}$ (c) with the condition $\Delta_{SO} \gg \Delta$, $\Delta_{exch} \geq 0$ in all cases. The upper indices L and U correspond to the lower and upper exciton states with the same F as was first introduced in Ref. [44]. Values of Δ and Δ_{exch} scale differently with the radius in spherical NCs resulting in the size dependence of exciton energy-level splitting [44].

The shape and size of NCs even more affect the exciton fine-energy structure in the external magnetic field. Figure 8 shows schematically the Zeeman splitting of exciton levels in a weak magnetic field $\mu_B B \ll \Delta_{exc}$ [$\mu_B B \ll \Delta$ in Figs. 8(a) and 8(c)] when the field-induced mixing of exciton states can be neglected. If the field direction is tilted by the angle Θ with respect to the anisotropy axis (if $\Delta \neq 0$), the Zeeman splitting of exciton states with opposite sign of $F \neq 0$ is $\propto \cos \Theta$.

It is convenient to define the effective g factor of the exciton state with $F \neq 0$ as

$$g_{ex,|F|} = \frac{E_{|F|} - E_{-|F|}}{\mu_B B_z}. \quad (18)$$

With such defined g factors, the exciton Zeeman splittings depicted in Fig. 8 can be written as $\Delta E_{ex,|F|} = g_{ex,|F|} \mu_B B \cos \Theta$. It is often the dark (optically spin-forbidden) exciton with $F = \pm 2$ which is addressed by the magneto-optical experiments such as the studies of the circularly polarized PL at low temperature [23,55,103,104]. The heavy-hole g factor can be obtained as $g_{h,3/2} = (g_e - g_{ex,2})/3$ ($g_{h,3/2} \equiv g_h^{sph}$ in spherical NCs). The evaluation of the dark exciton g factor $g_{ex,2}$ from the magnetic field dependence of the DCP in ensemble measurements and consequent estimation of the hole g factor is complicated by the influence of additional factors related to different mechanisms of the activation of the dark exciton recombination and different mechanisms of the exciton thermalization [55,104].

These uncertainties are overcome in single NC studies, which allow directly to observe the Zeeman splitting of the dark exciton. In Ref. [20] for CdSe/ZnS NCs with 4-nm core radius $g_{ex,2} = 2.7$ was determined. Using the electron g factor ≈ 0.9 , hole g factor $g_h = -0.6$ can be estimated. Note that both the electron and hole g factors in the core/shell structure can be affected by the carried leakage into the shell.

The g factors of the bright excitons with $F = \pm 1$ depend strongly on the ratio between Δ and Δ_{exch} and thus on the shape and size of NC. In thin NPLs, for example, made of zb-CdSe, the case $\Delta_{SO} \gg \Delta \gg \Delta_{exch}$ is realized and the Zeeman splittings of the bright excitons 1^L and 1^U in low magnetic fields $\mu_B B \ll \Delta_{exch}$ [see Fig. 8(a)] are described by $g_{ex,1}^L \equiv g_1^{hh} = -(g_e + 3g_{h,3/2})$ and $g_{ex,1}^U \equiv g_1^{lh} = g_e - g_{h,1/2}$ [compare with Eq. (17)]. The bright heavy-hole exciton g factor in ensembles of oriented CdSe NPLs was recently studied by the circular dichroism in high magnetic field [105]. Using reported g_1^{hh} values and the electron g -factor size dependence [see Fig. 11(b)] for NPLs with large in-plane sizes we estimate $g_{h,3/2} = -(g_e + g_1^{hh})/3$ in the range $-0.8 \div -0.6$ for 3-, 4-, and 5-ML-thick bare-core NPLs with the decrease of the absolute values with NPL thickness increase. Such a tendency is in agreement with our calculations for NPLs with parabolic confining potential [curves for the 2D limit and $30 \times 30 \text{ nm}^2$ NPL in Figs. 7(a) and 7(c)], although the absolute values are

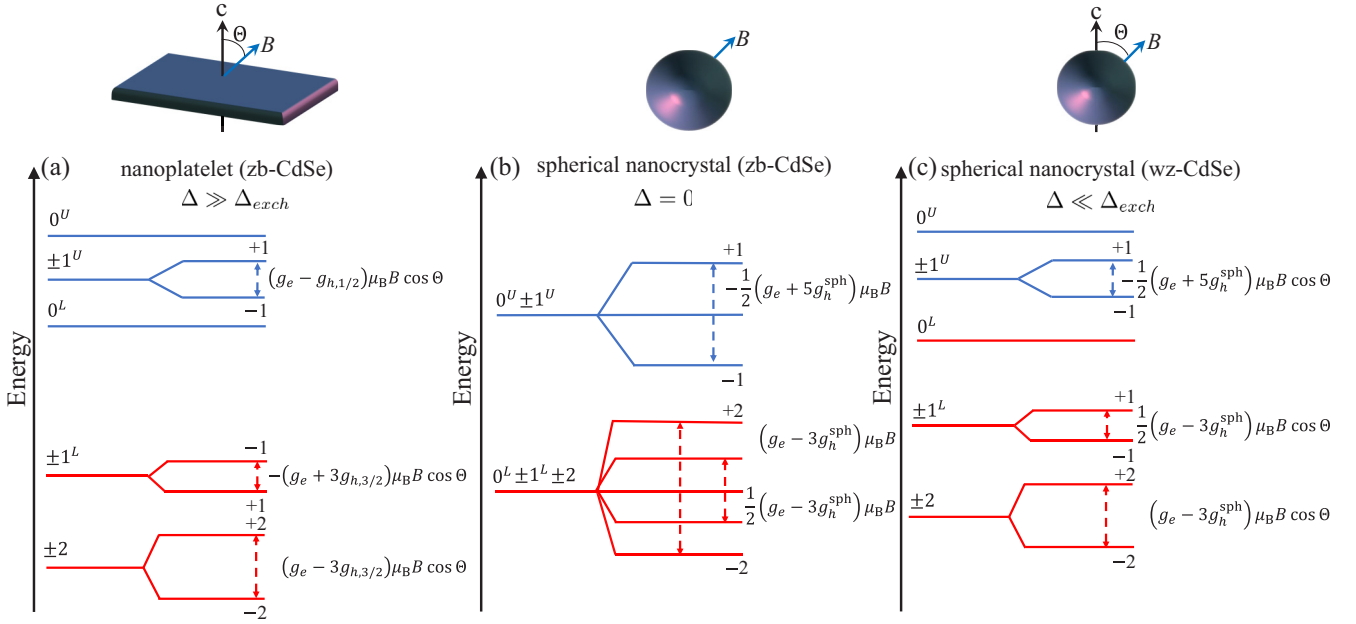


FIG. 8. Scheme of the exciton energy levels in magnetic field $\mu_B B \ll \Delta_{exch} \ll \Delta_{SO}$ for (a) $\Delta_{exch} \ll \Delta \ll \Delta_{SO}$; (b) $\Delta = 0$; (c) $\mu_B B \ll \Delta \ll \Delta_{exch}$. All resulting g factors are assumed to be positive, Θ is the angle between anisotropy axis and magnetic field. The order of energy levels is sketched for $g_e = 1.7$, $g_h^{sph} = -0.7$, $g_{h,3/2} = -0.1$, $g_{h,1/2} = 0.1$.

larger and close to the values calculated with a relatively small lateral area similar to NPLs used in experiment. The decrease of g_1^{hh} (positive) values with the decrease of the lateral sizes reported in [105] is related to the increase of the electron g factor.

In the general case, the electron-hole exchange interaction leads to the additional mixing of excitons formed with heavy, light, and spin-orbit-split holes confined in spheroidal and cuboidal NCs and the Zeeman splittings of the 1^L and 1^U excitons are controlled by the g factors $g_{ex,1}^{L,U}$ which are linear combinations of g_1^{hh} and g_1^{lh} . In spherical NCs, limiting cases with $\Delta = 0$, $\Delta_{exch} \ll \Delta_{SO}$ (in zb-CdSe) or $\Delta \ll \Delta_{exch} \ll \Delta_{SO}$ (in wz-CdSe) can be realized as shown in Figs. 8(a) and 8(b). In these cases the expressions for the exciton g factors are simplified to [54]

$$\begin{aligned} g_{ex,1}^L &= \frac{1}{4}g_1^{hh} + \frac{3}{4}g_1^{lh} = \frac{1}{2}(g_e - 3g_h^{sph}) \equiv \frac{1}{2}g_{ex,2}, \\ g_{ex,1}^U &= \frac{3}{4}g_1^{hh} + \frac{1}{4}g_1^{lh} = -\frac{1}{2}(g_e + 5g_h^{sph}). \end{aligned} \quad (19)$$

The Zeeman splitting of the bright excitons in ensemble of CdSe NCs was also addressed by studying the magnetic circular dichroism [17]. The observed g factors were considered as the effective exciton g factor g_{eff} averaged between lower and upper exciton g factors with the probabilities of their optical excitation. Unfortunately, the size-independent bulk value of the electron g factor $g_e = 0.68$ was used in [17] to obtain $g_h = -1.04$ and $g_h = -0.76$ from $g_{eff} = 1.424$ and $g_{eff} = 1.004$ in bare core wz-CdSe NCs with radius 2.5 and 1.9 nm, respectively. In the limit $\Delta \ll \Delta_{exch}$ the 1^L exciton is almost dark and we obtain with Eq. (7) in [17] $g_{eff} \approx 2g_{ex,1}^U/3$. With electron g -factor size dependence from Fig. 10 we recalculate $g_h \approx -1.01$ (-0.87) for 2.5 (1.9) NCs nm. These values are close to those calculated. However, the opposite size dependence of the resulting hole g factor demonstrates

that for the proper analysis of the hole g -factor size dependence from the data measured on exciton one needs to take into account both size dependence of the electron g factor and of the zero-field exciton fine structure, which is beyond the scope of this paper.

The Zeeman splitting of the bright exciton can be measured under the selective excitation in the spin-flip Raman scattering or fluorescence line narrowing (FLN) experiment. The Zeeman splitting of the lowest bright exciton in CdSe NCs was directly observed in the FLN in high magnetic field up to 60 T

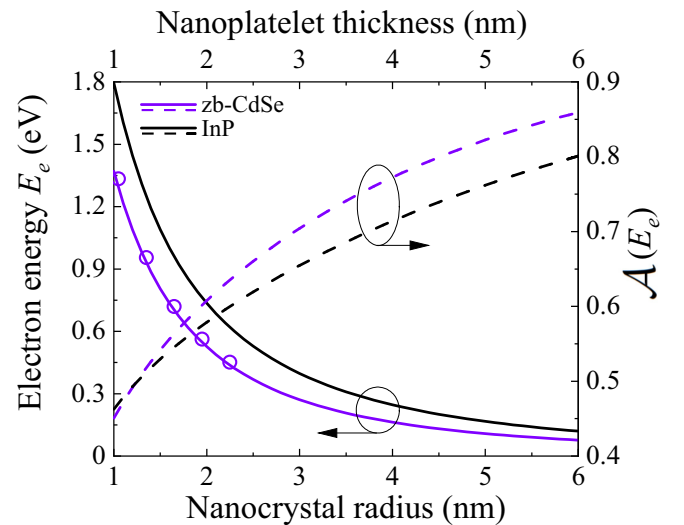


FIG. 9. Size dependencies of the electron energy E_e (solid lines, left axis) and renormalization constant $\mathcal{A}(E_e)$ (dashed lines, right axis) in zb-CdSe and InP nanocrystals. Open circles show the results of the tight-binding calculations for zb-CdSe NPLs from [112].

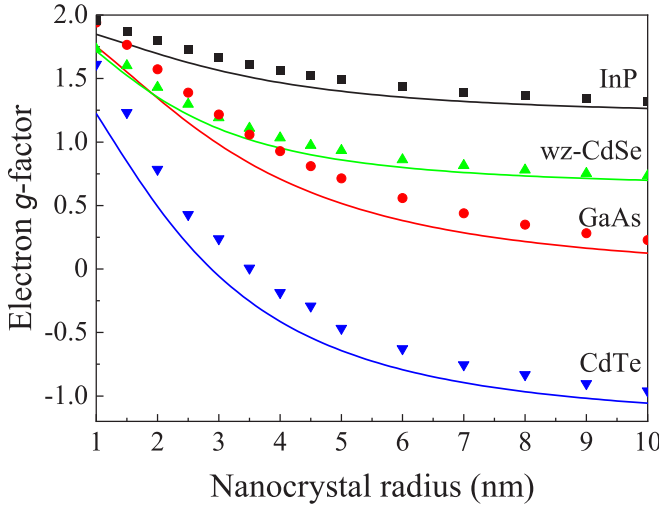


FIG. 10. Size dependencies of the electron g factor in different semiconductors calculated within tight-binding approach [29] (symbols) and using the eight-band $\mathbf{k} \cdot \mathbf{p}$ [Eq. (A5)] with the same sets of parameters listed in Table II.

[106,107] and of the upper bright exciton in InP/ZnSe NCs [108]. The analysis of the data at such high magnetic fields requires accounting of the field-induced mixing of the lower and upper excitons as it was done in [108] to obtain the hole g factor $g_h = -1.9$ for InP/ZnSe NCs with InP core diameter 3.2 nm. This value is quite close to the value calculated in this work within the six-band model for small InP NCs with the infinite boxlike potential [see Fig. 4(b)] while the four-band model predicts much smaller absolute value of the hole g factor.

VI. CONCLUSION

We show that in spherical and cube semiconductor NCs the admixture of the spin-orbit split-off Γ_7 valence subband state results in the size-dependent hole g factor and its account is important for the actual range of NC sizes. At the same time, the heavy-hole g -factor dependence on the NPL thickness is relatively weak for thin NPLs with large in-plane size. We have found that the heavy-hole g -factor significantly depends on the NPL lateral sizes for the realistic CdSe NPLs due to the effective admixture of the light hole and spin-orbit split-off hole states by the confining potential.

Our calculations demonstrate that results of the g -factor calculations obtained for zinc-blende semiconductors are applicable also for NCs made of semiconductors with the wurtzite crystal structure if the crystal field-induced splitting between light and heavy holes is much smaller than Δ_{SO} and the hole size quantization energy. At the same time, the uniaxial shape anisotropy in spheroidal NCs not only splits the heavy- and light-hole states, but results in the difference of their g factors.

We have demonstrated that the orbital contribution to the renormalization of the hole g factor in NCs as compared with the bulk value plays an important role for all considered NC shapes. Orbital contribution as a whole and the effect of the Γ_7 holes admixture in size dependence of the hole g factor

are more substantial in semiconductors with small β and a large value of γ_1 Luttinger parameter (smaller hole effective mass). We show that in cube NCs, the Zeeman splitting of the fourfold-degenerate hole state with momentum $\frac{3}{2}$ is nonequidistant as a consequence of breaking the rotational symmetry. This finding calls for further experimental studies.

ACKNOWLEDGMENTS

We thank D. R. Yakovlev and M. M. Glazov for valuable discussions. This work was funded by the Russian Science Foundation (Grant No. 20-42-01008).

APPENDIX A: SIZE DEPENDENCE OF THE ELECTRON ENERGY LEVEL AND EFFECTIVE g FACTOR IN THE EIGHT-BAND KANE MODEL

The eight-band Kane or $\mathbf{k} \cdot \mathbf{p}$ model allows one to account for the effect of the electron localization in low-dimensional structures on the g -factor value [25,26,109]. It results in the dependence of the electron g factor on the electron size quantization energy E_e counted from the bottom of the conduction band as

$$g_e(E_e) = g_0 + \int [\tilde{g}_e(E_e) - g_0] |\Psi_e^c(\mathbf{r})|^2 d^3\mathbf{r} + g_{\text{sur}}, \quad (\text{A1})$$

$$\tilde{g}_e(E_e) \approx g_0 + g_{\text{rb}} - \frac{2E_p}{3} \left(\frac{1}{\tilde{E}_g} - \frac{1}{\tilde{E}_g + \Delta_{SO}} \right). \quad (\text{A2})$$

Here $\tilde{E}_g = E_g + E_e$, $\Psi_e^c(\mathbf{r})$ describes the conduction band contribution to the eight-band electron envelope function $\Psi_e(\mathbf{r})$, and g_{sur} describes the surface/interface contribution proportional to the squared value $|\Psi_e^c|_{\text{sur}}^2$ taken at the surface of the nanostructure or at the interface between two semiconductors in the heterostructure [26].

The normalization condition for the total electron wave function $\Psi_e = \Psi_e^c + \Psi_e^v$, where $\Psi_e^v(r)$ describes the valence band contribution, reads as $\int |\Psi_e(\mathbf{r})|^2 d^3\mathbf{r} = \int (|\Psi_e^c(\mathbf{r})|^2 + |\Psi_e^v(\mathbf{r})|^2) d^3\mathbf{r} = 1$. Using the expression of $\Psi_e^v(\mathbf{r})$ via $\Psi_e^c(\mathbf{r})$ [110,111] one can rewrite the normalization condition as

$$\int |\Psi_e(\mathbf{r})|^2 d^3\mathbf{r} = \int |\Psi_e^c(\mathbf{r})|^2 \mathcal{A}^{-1}(E_e) d^3\mathbf{r} = 1, \quad (\text{A3})$$

$$\mathcal{A}(E_e) = [1 + \alpha_p(E_e)E_e m_e(E_e)/m_0]^{-1}.$$

Here $m_e(E_e)$ is the electron effective mass at the energy E_e and $\alpha_p(E_e) = m_0 \partial m_e^{-1}(E_e) / \partial E_e$ describes the nonparabolicity effect:

$$m_e(E_e) = m_0 \left[\gamma_{\text{rb}} + \frac{E_p}{3} \left(\frac{2}{\tilde{E}_g} + \frac{1}{\tilde{E}_g + \Delta_{SO}} \right) \right]^{-1},$$

$$\alpha_p(E_e) = \frac{E_p}{3} \left(\frac{2}{\tilde{E}_g^2} + \frac{1}{(\tilde{E}_g + \Delta_{SO})^2} \right). \quad (\text{A4})$$

Here γ_{rb} takes into account the contribution of remote bands. In semiconductor heterostructure, the electron effective mass in (A3) as well as the electron effective g factor $\tilde{g}_e(E_e)$ in (A1) can be different in different materials. In bare NCs, \mathcal{A} does not depend on the coordinate and can be directly used as the renormalization constant for the conduction band

TABLE II. Parameters for calculation of electron g factor: E_g is the energy gap, E_p is the Kane energy, Δ_{SO} is the spin-orbit energy, g_e and m_e/m_0 are bulk electron g factor and effective mass. For a comparison with tight-binding model calculation for wz-CdSe, CdTe, GaAs, InP we use set of parameters from Ref. [29], except electron effective masses. The second set of parameters for wz-CdSe is taken from Refs. [35,66]. For zb-CdSe we use set of parameters from Ref. [34].

Semiconductor	E_g (eV)	E_p (eV)	Δ_{SO} (eV)	g_e	g_e (expt.)	m_e/m_0
wz-CdSe	1.8174	21.40	0.3871	0.633	0.68 [35]	0.13 [74]
wz-CdSe	1.84	17.5	0.42	0.68 [35]		0.11
zb-CdSe	1.764	18.3	0.47	0.42	0.42 [34]	0.13
CdTe	1.611	19.57	0.8221	-1.236	-1.66 [36]	0.09 [74]
GaAs	1.519	25.34	0.3399	-0.065	-0.44 [33]	0.067 [113]
InP	1.424	20.45	0.108	1.22	1.2 [36]	0.08 [113]

contribution. At small energies $E_e \ll E_g$, one can approximate $m_e^{-1}(E) \approx m_e^{-1} - m_0^{-1} \alpha_p|_{E_e=0} E_e$, where $m_e \equiv m_e|_{E_e=0}$ is the electron effective mass at the bottom of the conduction band, and $\mathcal{A}(E_e) \approx m_e/m_e(E_e)$ [111].

Combining together Eqs. (A1) and (A2) we arrive to

$$g_e(E_e) = g_0[1 - \mathcal{A}(E_e)] + \tilde{g}_e(E_e)\mathcal{A}(E_e) + g_{\text{sur}} \quad (\text{A5})$$

for the bare-core NCs. Equation (A5) allows one to calculate the electron g factor in NCs knowing the bulk parameters E_p , E_g , Δ_{SO} , m_e , g_e and the surface contribution g_{sur} .

In Ref. [26] it was discussed that the surface contribution g_{sur} to the electron g factor can be nonzero even for the bare NC with the infinite potential barrier at the surface. However, we consider below the case of the vanishing electron conduction band wave-function component at the surface $\Psi_e^c(\mathbf{r})|_{r=s} = 0$ corresponding to $g_{\text{sur}} = 0$. In this case, Eq. (A5) gives the universal dependence of the electron g factor on the electron energy E_e (not the optical transition energy) within the eight-band $\mathbf{k} \cdot \mathbf{p}$ model valid for any NC potential shape. The size dependence of the electron g factor can be found by establishing the correspondence between the electron quantization energy E_e and the size of the NC of a particular shape.

For spherical NCs of the radius a , the equation for the ground state $1S_e$, electron quantization energy under assumption of zero boundary condition $\Psi_e^c(a) = 0$ reads as

$$E_e = \frac{\hbar^2 \pi^2}{2m_e(E_e)a^2}. \quad (\text{A6})$$

It can be solved numerically for E_e at a given a to obtain $g_e(E_e(a))$. Alternatively, one can use the electron energy E_e to obtain the parametrized dependence $g_e(a)$ [Eqs. (A5) and (A6)]. Figure 9 shows the size dependencies of the electron energy E_e (solid lines, left axis) and the renormalization constant $\mathcal{A}(E_e)$ (dashed lines, right axis) in zb-CdSe and InP nanocrystals. The electron energies calculated according to Eq. (A6) are in a good agreement with the results of the tight-binding calculations for zb-CdSe NPLs from [112]. One can see that in small NCs the renormalization $\mathcal{A}(E_e)$ can be as small as 0.5, resulting in additional corrections to the electron g factor, up to 10% as compared with Eq. (A2). It is also possible to calculate the electron g factor for the excited nS_e states in spherical NCs using Eq. (A5) and factor n^2 in Eq. (A6). The size dependencies of the electron energy level, effective mass, and effective g factor in a QW or NPL with

infinite in-plane sizes and the thickness L can be obtained after the replacement of nanocrystal radius a by the well width L in Eq. (A6). The calculation of the electron g factor for NPLs with a finite lateral cross section is beyond the scope of this paper as the electron effective mass could be anisotropic, complicating the analysis.

We show in Fig. 10 that the eight-band $\mathbf{k} \cdot \mathbf{p}$ calculations of the electron g factor, according to Eq. (A5), provide a good agreement with results of the tight-binding calculations [29] for spherical NCs made from wz-CdSe, CdTe, GaAs, and InP. We used in Fig. 10 the same set of bulk parameters for the $\mathbf{k} \cdot \mathbf{p}$ calculations obtained by the tight-binding calculations in [29] (see Table II).

In Fig. 11 the dependencies of the electron g factor on the radius of wz-CdSe and zb-CdSe nanocrystals calculated according to Eq. (A5) are shown by the green and violet solid lines, respectively. Calculations are made with the set of parameters from Refs. [35,66] and $g_{\text{rb}} = 0.02$ for wz-CdSe and from Ref. [34] and $g_{\text{rb}} = -0.125$ for zb-CdSe, correspondingly, and $g_{\text{sur}} = 0$. Dashed lines show the calculations according to Eq. (A2). One can see that the difference between solid, $g_e(E_e)$, and dashed, $\tilde{g}_e(E_e)$, lines increases with decreasing of NC size related to the $\mathcal{A}(E_e)$ effect while the difference between g factors calculated for zb- and wz-CdSe decreases.

In Fig. 11 we show also the values of the g factors measured by the pump-probe Faraday rotation experiment in Refs. [18,99] for wz-CdSe (g_1 and g_2 values) and in Ref. [114] for zb-CdSe. The typical experimental error of the measuring g factors is about ± 0.01 . Calculated $g_e(E_e)$ dependence for wz-CdSe is in a good agreement with the experimental g_1 data shown by filled red and blue circles and attributed to the ground-state electron g factor. A good agreement of the calculated size dependence of the electron g factor with experiment can be achieved with more than one set of $\mathbf{k} \cdot \mathbf{p}$ model parameters. In Refs. [18,26] another set of parameters was used together with the general boundary condition with a nonvanishing electron wave function at NC surface resulting in $g_{\text{sur}} \neq 0$.

It is noteworthy that the second set of experimental data for wz-CdSe, g_2 values given by open symbols in Fig. 11(a), can not be described by the calculated dependence for electron g factor at lowest quantum size level $1S_e$. In literature, there were different assignments of these values to the exciton g factor [18,101], anisotropic g factor of electron [28], for wz-CdSe and to the electron g factor for zb-CdSe [114]. Considering the exciton hypothesis it is necessary to use the proper relation

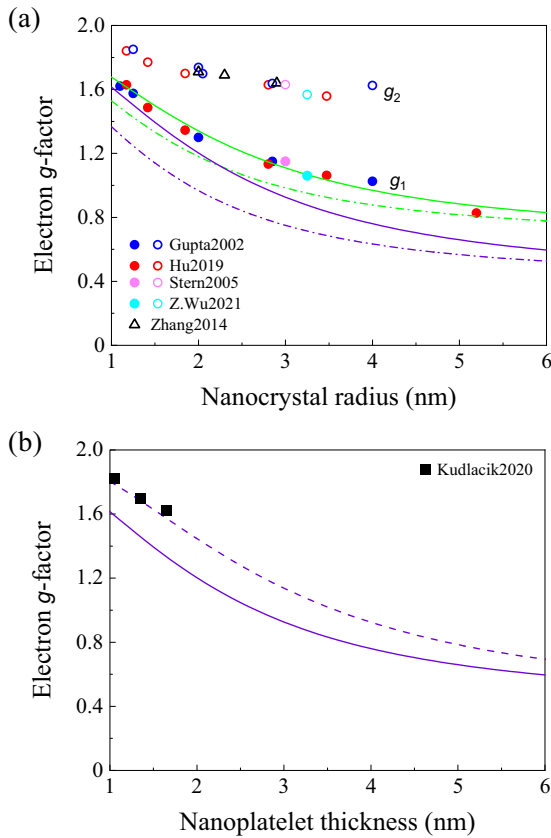


FIG. 11. Size dependence of electron g factor: (a) in spherical wz- (green lines) and (purple) zb-CdSe NCs. Solid (dashed) lines correspond to the infinite boxlike potential according to Eq. (A5) [Eq. (A2)] with parameters from Refs. [35,66] and [34] for wz-CdSe and zb-CdSe. Circles correspond to g factors observed via the pump-probe Faraday rotation in wz-CdSe NCs (blue [18], red [99], cyan [100], magenta [101]). Black triangles denote experimental data for zb-CdSe NCs [114]; (b) in zb-CdSe NPLs with infinite lateral sizes calculated for the infinite boxlike (dashed line) and parabolic (solid line) potential. Black squares denote the resident electron g factors in zb-CdSe NPLs measured via the SFRS [98].

between the exciton g factor and Larmor frequency which is given for the particle with the total spin S by $\hbar\Omega = g\mu_B B/2S$. Using the definition (18) for the g factor of the bright exciton with momentum projection $|F = 1\rangle$, one obtains $g_1^L(\Delta = 0) = 2g_2$ [or $g_1^U(\Delta = 0) = 2g_2$ with $g_1^{L,U}(\Delta = 0)$ given by Eq. (19)] instead of $g_1^L(\Delta = 0) = g_2$ suggested in [18]. In this case, to describe the size dependence of g_2 in Fig. 11(a) as $g_2 = g_1^L(\Delta = 0)/2$ one has to use $g_h \approx -1.8$ instead of -0.73 obtained in [18]. The value $g_h \approx -1.8$ is too large as compared with our theoretical estimations given in this paper even with account of the admixture from the spin-orbit-split valence band in small NCs making doubtful interpretation of g_2 as the g factor of $|1^L\rangle$ exciton. Alternatively, the g_2 -related precession could be ascribed to $|1^U\rangle$ exciton in quasispherical NCs with $\Delta = 0$. In this case, the size-dependent hole g factor changing from -1.4 in 8-nm NCs to -1.7 in 3-nm NCs allows to fit the $g_2 = g_1^U(\Delta = 0)/2$ dependence. Again, these hole g -factor values are larger than our calculated results and published experimental data. In two recent papers [99,100]

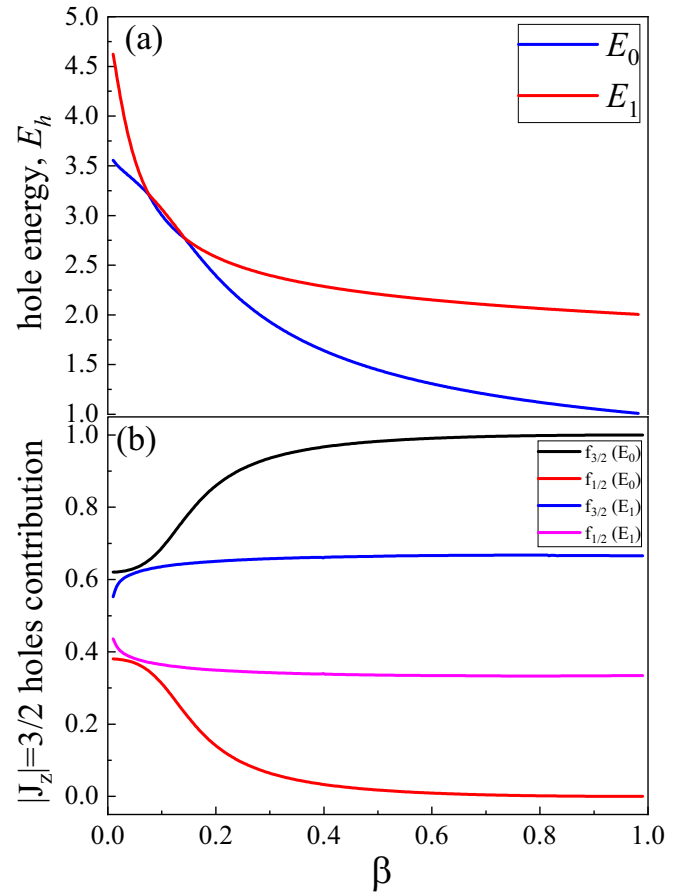


FIG. 12. (a) The dependence of first two hole states energies E_0 and E_1 in cube nanocrystals on the effective mass ratio β in zero magnetic field. Energies are given in units $E_h = 3\hbar^2\pi^2/2m_{hh}L^2$, L being nanocrystal size (cube width). (b) The heavy-hole contributions as function of β for the hole states originating from the ground and first excited states.

the interpretation of the g_2 as the surface-localized electron g factor was proposed. The calculations of such electrons g factor are beyond the scope of this paper.

Recently, the g factor of the localized resident electron was measured in zb-CdSe nanoplatelets with thickness of 3, 4 and 5 ML by the spin-flip Raman scattering (SFRS) [98]. The attribution of the obtained g factors to the resident electron is justified by the polarization selection rules [98,115]. In Fig. 11(b) the measured g factors are given by black squares. The solid and dashed lines are results of the calculations according to Eq. (A5) for electrons in the NPLs with the parabolic and boxlike confining potentials, respectively. We remind, that, we define here the NPL width L of the nanocrystals with parabolic potential as $L = 4L_e$, where L_e is the oscillator length calculated with the electron effective mass at the bottom of conduction band. One can see that the parabolic potential better describes the experimental data while the measured g factors are about 10% larger than calculated for the boxlike potential. However, the discrepancy can be related to the effect of the g -factor anisotropy in the NPL neglected in the presented calculations as well as to the effect of the additional in-plane localization of the resident electron.

**APPENDIX B: MAGNETIC FIELD PERTURBATION
TO THE HOLE HAMILTONIAN**

The orbital Bloch functions of the top of valence band in studied semiconductors are of p -like symmetry and are often designated as X , Y , and Z , each having two possible spins, \uparrow and \downarrow [49,68]. Taking into account spin-orbit interaction leads to the splitting of the valence band with the following set of functions being the basis of the topmost Γ_8 and spin-split Γ_7 subbands [49,68]:

$$\begin{aligned} \left| \Gamma_8, +\frac{3}{2} \right\rangle &= -\uparrow \frac{X + iY}{\sqrt{2}}, \\ \left| \Gamma_8, +\frac{1}{2} \right\rangle &= \sqrt{\frac{2}{3}} \uparrow Z - \downarrow \frac{X + iY}{\sqrt{6}}, \end{aligned}$$

$$\begin{aligned} \left| \Gamma_8, -\frac{1}{2} \right\rangle &= \sqrt{\frac{2}{3}} \downarrow Z + \uparrow \frac{X - iY}{\sqrt{6}}, \\ \left| \Gamma_8, -\frac{3}{2} \right\rangle &= \downarrow \frac{X - iY}{\sqrt{2}}, \\ \left| \Gamma_7, +\frac{1}{2} \right\rangle &= \frac{1}{\sqrt{3}} \uparrow Z + \downarrow \frac{X + iY}{\sqrt{3}}, \\ \left| \Gamma_7, -\frac{1}{2} \right\rangle &= -\frac{1}{\sqrt{3}} \downarrow Z + \uparrow \frac{X - iY}{\sqrt{3}}. \end{aligned} \quad (\text{B1})$$

Each of the Γ_8 functions (B1) have momentum $\frac{3}{2}$ and its projection on the z axis $\pm\frac{3}{2}$ and $\pm\frac{1}{2}$, Γ_7 functions have full momentum $\frac{1}{2}$ and its projection on the z axis $\pm\frac{1}{2}$.

The hole six-band Hamiltonian of Eq. (4) can be written in a matrix form in the basis (B1) as follows [49,68]:

$$\hat{H} = \frac{\hbar^2}{2m_0} \begin{pmatrix} P+Q & -S & R & 0 & -\frac{1}{\sqrt{2}}S & \sqrt{2}R \\ -S^* & P-Q & 0 & R & -\sqrt{2}Q & \sqrt{\frac{3}{2}}S \\ R^* & 0 & P-Q & S & \sqrt{\frac{3}{2}}S^* & \sqrt{2}Q \\ 0 & R^* & S^* & P+Q & -\sqrt{2}R^* & -\frac{1}{\sqrt{2}}S^* \\ -\frac{1}{\sqrt{2}}S^* & -\sqrt{2}Q & \sqrt{\frac{3}{2}}S & -\sqrt{2}R & P+\bar{\Delta} & 0 \\ \sqrt{2}R^* & \sqrt{\frac{3}{2}}S^* & \sqrt{2}Q & -\frac{1}{\sqrt{2}}S & 0 & P+\bar{\Delta} \end{pmatrix}, \quad \begin{aligned} P &= \gamma_1(k_x^2 + k_y^2 + k_z^2), & Q &= \gamma(k_x^2 + k_y^2 - 2k_z^2), \\ R &= -\sqrt{3}\gamma(k_x - ik_y)^2, & S &= 2\sqrt{3}\gamma k_z(k_x - ik_y), \\ \bar{\Delta} &= \frac{2m_0}{\hbar^2} \Delta_{\text{SO}}. \end{aligned} \quad (\text{B2})$$

In the external magnetic field, the hole wave vector \mathbf{k} has to be renormalized as $\mathbf{k} \rightarrow \mathbf{k} - \frac{e\mathbf{A}}{c\hbar}$, where \mathbf{A} is the vector potential of magnetic field. The case $\mathbf{B} \parallel z$ in the Landau gauge corresponds to $\mathbf{A} = (0, Bx, 0)$. The B -linear correction to the hole Hamiltonian (4) is (in the units of $\mu_B B$)

$$\hat{H}_B = \begin{pmatrix} P_B + Q_B & -S_B & R_B & 0 & -\frac{1}{\sqrt{2}}S_B & \sqrt{2}R_B \\ -(S_B)^\dagger & P_B - Q_B & 0 & R_B & -\sqrt{2}Q_B & \sqrt{\frac{3}{2}}S_B \\ (R_B)^\dagger & 0 & P_B - Q_B & S_B & \sqrt{\frac{3}{2}}(S_B)^\dagger & \sqrt{2}Q_B \\ 0 & (R_B)^\dagger & (S_B)^\dagger & P_B + Q_B & -\sqrt{2}(R_B)^\dagger & -\frac{1}{\sqrt{2}}(S_B)^\dagger \\ -\frac{1}{\sqrt{2}}(S_B)^\dagger & -\sqrt{2}Q_B & \sqrt{\frac{3}{2}}S_B & -\sqrt{2}R_B & P_B & 0 \\ \sqrt{2}(R_B)^\dagger & \sqrt{\frac{3}{2}}(S_B)^\dagger & \sqrt{2}Q_B & -\frac{1}{\sqrt{2}}S_B & 0 & P_B \end{pmatrix}, \quad \begin{aligned} P_B &= \gamma_1(-2xk_y), \\ Q_B &= \gamma(-2xk_y), \\ R_B &= -\sqrt{3}\gamma(1 + 2ixk_x + 2xk_y), \\ (R_B)^\dagger &= -\sqrt{3}\gamma(-1 - 2ixk_x + 2xk_y), \\ S_B &= 2\sqrt{3}i\gamma xk_z, \\ (S_B)^\dagger &= -2\sqrt{3}i\gamma xk_z. \end{aligned} \quad (\text{B3})$$

In the same units the Zeeman Hamiltonian (5) in the basis (B1) has the form

$$\hat{H}_Z = \begin{pmatrix} -3\kappa & 0 & 0 & 0 & 0 & 0 \\ 0 & -\kappa & 0 & 0 & \sqrt{2}\kappa + \sqrt{2} & 0 \\ 0 & 0 & \kappa & 0 & 0 & \sqrt{2}\kappa + \sqrt{2} \\ 0 & 0 & 0 & 3\kappa & 0 & 0 \\ 0 & \sqrt{2}\kappa + \sqrt{2} & 0 & 0 & -2\kappa - 1 & 0 \\ 0 & 0 & \sqrt{2}\kappa + \sqrt{2} & 0 & 0 & 2\kappa + 1 \end{pmatrix}, \quad (\text{B4})$$

which contains nondiagonal matrix elements.

Now we obtain Eq. (14) from the main text as a first order on magnetic field correction to the hole Hamiltonian. We consider a 2D structure with infinite in-plane size, so that $k_x = k_y \equiv 0$ and $k_z \neq 0$. The zero-order hole Hamiltonian in zero magnetic field is obtained from Eq. (B2) with

setting $k_x = k_y \equiv 0$ and adding nanostructure potential $V(z)$ on diagonal. The off-diagonal matrix elements mix hole states with $J = \frac{3}{2}$, $J_{hz} = \pm\frac{1}{2}$ (light holes) and $J = \frac{1}{2}$, $J_{hz} = \pm\frac{1}{2}$ (spin-split holes). Note that the Zeeman part \hat{H}_Z does not contribute to the heavy-hole g -factor renormalization in such structures.

To use the perturbation theory, one has to diagonalize Hamiltonian (B2) with $k_x = k_y \equiv 0$. In the general case this has to be made numerically, while for the boxlike infinite potential $V(z)$ the calculation can be made analytically. In the case of the boxlike potential matrix elements, $Q = -2k_z^2$ mix only eigenstates of the light and Γ_7 holes with the same quantum number n . As a result, one can obtain the proper zeroth-order basis and perturbation Hamiltonian for states with a fixed n analytically and separately. Functions $F_{1,4} =$

$|\Gamma_8, \pm 3/2\rangle$ will remain unchanged while the other functions are

$$F_{2,3} = C_1|\Gamma_8, \pm 1/2\rangle \mp C_2|\Gamma_7, \pm 1/2\rangle, \quad (\text{B5})$$

$$F_{5,6} = \pm C_2|\Gamma_8, \pm 1/2\rangle + C_2|\Gamma_7, \pm 1/2\rangle$$

with $C_1^2 + C_2^2 = 1$. For the boxlike infinite potential, coefficients C_1 and C_2 are

$$C_1 = \frac{\beta + \sqrt{\beta^2(4\delta_{\text{SO}}^2 + 4\delta_{\text{SO}} + 9) - 2\beta(2\delta_{\text{SO}} + 9) + 9 + 2\beta\delta_{\text{SO}} - 1}}{\sqrt{8(\beta - 1)^2 + (\beta + \sqrt{\beta^2(4\delta_{\text{SO}}^2 + 4\delta_{\text{SO}} + 9) - 2\beta(2\delta_{\text{SO}} + 9) + 9 + 2\beta\delta_{\text{SO}} - 1})^2}}, \quad (\text{B6})$$

$$C_2 = \frac{2\sqrt{2}(1 - \beta)}{\sqrt{8(\beta - 1)^2 + (\beta + \sqrt{\beta^2(4\delta_{\text{SO}}^2 + 4\delta_{\text{SO}} + 9) - 2\beta(2\delta_{\text{SO}} + 9) + 9 + 2\beta\delta_{\text{SO}} - 1})^2}}, \quad (\text{B7})$$

where $\delta_{\text{SO}} = \Delta_{\text{SO}}/E_{hh_1}$, $E_{hh_1} = \hbar^2(\gamma_1 - 2\gamma)/2m_0L_z^2$. In limiting cases we have $\lim_{\delta_{\text{SO}} \rightarrow \infty} C_1 = 1$, $\lim_{\delta_{\text{SO}} \rightarrow 0} C_1 = 1/\sqrt{3}$, $\lim_{\delta_{\text{SO}} \rightarrow \infty} C_2 = 0$, $\lim_{\delta_{\text{SO}} \rightarrow 0} C_2 = \sqrt{2/3}$.

The new perturbation is $\hat{H}_B = M\hat{H}_B M^{-1}$,

$$M = \begin{pmatrix} 1 & 0 & 0 & 0 & 0 & 0 \\ 0 & C_1 & 0 & 0 & -C_2 & 0 \\ 0 & 0 & C_1 & 0 & 0 & C_2 \\ 0 & 0 & 0 & 1 & 0 & 0 \\ 0 & C_2 & 0 & 0 & C_1 & 0 \\ 0 & 0 & -C_2 & 0 & 0 & C_1 \end{pmatrix}. \quad (\text{B8})$$

Its matrix elements contributing to $g_{h,3/2}^{\text{2D}}$ in μB units are

$$(\hat{H}_B)_{12} = A_1(\delta_{\text{SO}}, \beta)S_B, \quad (\hat{H}_B)_{15} = A_2(\delta_{\text{SO}}, \beta)S_B,$$

$$(\hat{H}_B)_{43} = -A(\delta_{\text{SO}}, \beta)S_B^*, \quad (\hat{H}_B)_{46} = B(\delta_{\text{SO}}, \beta)S_B^*,$$

$$A_1(\delta_{\text{SO}}, \beta) \equiv A_2\left(\frac{\Delta_{\text{SO}}}{E_{hh_1}}, \beta\right) = \frac{C_2}{\sqrt{2}} - C_1,$$

$$A_2(\delta_{\text{SO}}, \beta) \equiv A_2\left(\frac{\Delta_{\text{SO}}}{E_{hh_1}}, \beta\right) = -\frac{C_1}{\sqrt{2}} - C_2$$

and the light-hole and Γ_7 hole state energies now depending both on β and δ_{SO} are given by

$$\begin{aligned} \tilde{E}_{lh_{2n}} &= \frac{2\hbar^2\pi^2n^2\gamma_1}{m_0L_z^2} \frac{(\beta\delta_{\text{SO}} + 2\beta n^2 + 6n^2 - \sqrt{\beta^2\delta_{\text{SO}}^2 + 36\beta^2n^4 - 72\beta n^4 + 36n^4 + 4\beta^2\delta_{\text{SO}}n^2 - 4\beta\delta_{\text{SO}}n^2})}{4(\beta + 1)}, \\ \tilde{E}_{\text{SO}_{2n}} &= \frac{2\hbar^2\pi^2n^2\gamma_1}{m_0L_z^2} \frac{(\beta\delta_{\text{SO}} + 2\beta n^2 + 6n^2 + \sqrt{\beta^2\delta_{\text{SO}}^2 + 36\beta^2n^4 - 72\beta n^4 + 36n^4 + 4\beta^2\delta_{\text{SO}}n^2 - 4\beta\delta_{\text{SO}}n^2})}{4(\beta + 1)}. \end{aligned} \quad (\text{B9})$$

Function $G(\beta)$ for the boxlike potential can be expressed in the first order on $1/\delta_{\text{SO}}$, $\delta_{\text{SO}} = \Delta_{\text{SO}}/E_{hh_1}$ as

$$G(\beta) = \sum_{n=1}^{\infty} \frac{192(\beta - 1)^2n^2}{\pi^2(\beta + 1)(4n^2 - 1)^2(n^2 - \beta)} + \frac{1}{\delta_{\text{SO}}} \sum_{n=1}^{\infty} \frac{192(\beta - 1)^2n^2[\beta(\beta + 1) + 2(\beta^2 - 2\beta + 2)n^4 - (3\beta + 1)n^2]}{\pi^2\beta(\beta + 1)(1 - 4n^2)^2(n^2 - \beta)^2}. \quad (\text{B10})$$

For the parabolic potential one can express analytically $G(\beta)$ only in the limit $\delta_{\text{SO}} \rightarrow \infty$:

$$G(\beta) = - \sum_{n=1}^{\infty} \frac{24\sqrt{\beta}(\sqrt{\beta} - 1)^{2n}(\sqrt{\beta} + 1)^{1-2n}\Gamma(n + \frac{1}{2})}{\sqrt{\pi}(\beta + 1)(\sqrt{\beta} - 4n + 1)\Gamma(n)}$$

with $\Gamma(x)$ being the Euler gamma function.

APPENDIX C: ELECTRON AND HOLE ENERGY LEVELS IN THE NANOCRYSTALS WITH CUBIC SHAPE

We consider NCs with the cubic shape and edges directed along the crystal axes. The potential of such NC is described by a rectangular potential with infinite barrier:

$$V^{\text{cube}}(x, y, z) = \begin{cases} 0, & |x|, |y|, |z| \leq \frac{L}{2} \\ \infty, & |x|, |y|, |z| > \frac{L}{2} \end{cases} \quad (\text{C1})$$

where x, y, z are electron or hole coordinates. The conduction band electron energy levels can be found from (A6) with $a \rightarrow L/\sqrt{3}$. With this substitution, the size dependence of the energy levels, effective mass, and effective g factors can be seen in Figs. 9 and 11.

For holes the situation is more complicated as the hole wave function is a six-component one. In order to calculate hole states in cube nanocrystal we developed a numerical method. The hole kinetic energy is described by the Hamiltonian (4) and the NC potential is taken from Eq. (C1). The potential (C1) mixes hole states with different spin projections J_z and, unlike the spherically symmetric case, due to lower symmetry the Schrödinger equation of the hole can not be simplified (compare with Refs. [66,70]). We numerically diagonalize the hole Hamiltonian matrix calculated on the six-component basis of eigenfunctions of infinite rectangular

quantum well along coordinate axes:

$$\Psi_{J_x, J_y, J_z}^{n_x, n_y, n_z}(x, y, z) = \phi^{n_x}(x)\phi^{n_y}(y)\phi^{n_z}(z),$$

$$\phi^{n_\alpha}(\alpha) = \sqrt{\frac{2}{L}} \sin\left[\frac{\pi n_\alpha}{L}\left(\alpha + \frac{L}{2}\right)\right], \quad (\text{C2})$$

where $J = \frac{3}{2}, \frac{1}{2}$, $J_z = \pm\frac{3}{2}, \pm\frac{1}{2}$, $n_x, n_y, n_z = 1, \dots, N$, and $\alpha = x, y, z$. All matrix elements are calculated analytically and basis size is $N = 16$, which is more than enough to obtain convergence for several lowest hole states at any reasonable value of β .

The dependencies of the energies of the two lowest hole states on β in the limit $\Delta_{SO}/E_h \rightarrow \infty$ are shown in Fig. 12(a). We emphasize the crossing of the levels E_0 and E_1 leading to level E_1 being the ground state in some range of β . This leads to the significant change of the hole ground-state structure in the vicinity of the crossing point. In Fig. 12(b) we show the heavy-hole ($|J_z| = \frac{3}{2}$) contributions to hole wave function $f_{|M|}$ as function of β for states, corresponding to energy levels E_0 and E_1 . For rather large β and far from crossing the ground state is the S -like state E_0 and $\frac{3}{2}$ hole states are mostly formed from heavy holes and $\frac{1}{2}$ states are mostly light holes. On the opposite, for smaller β , in crossing range or near its levels E_0 and E_1 are close to each other and, consequently, are strongly mixed. As a result, the contributions of heavy and light holes to the ground-state sublevels are comparable, leading to the specific features in dependencies of the hole g factors on β .

-
- [1] Alexander L. Efros and Louis E. Brus, Nanocrystal quantum dots: From discovery to modern development, *ACS Nano* **15**, 6192 (2021).
- [2] Celso de Mello Donegá, Synthesis and properties of colloidal heteronanocrystals, *Chem. Soc. Rev.* **40**, 1512 (2011).
- [3] S. Ithurria and B. Dubertret, Quasi 2d colloidal CdSe platelets with thicknesses controlled at the atomic level, *J. Am. Chem. Soc.* **130**, 16504 (2008).
- [4] M. V. Kovalenko, L. Manna, A. Cabot, Z. Hens, D. V. Talapin, C. R. Kagan, V. I. Klimov, A. L. Rogach, P. Reiss, D. J. Milliron, Ph. Guyot-Sionnest, G. Konstantatos, W. J. Parak, T. Hyeon, B. A. Korgel, C. B. Murray, and W. Heiss, Prospects of nanoscience with nanocrystals, *ACS Nano* **9**, 1012 (2015).
- [5] D. Graham-Rowe, From dots to devices, *Nat. Photonics* **3**, 307 (2009).
- [6] S. E. Lohse and C. J. Murphy, Applications of colloidal inorganic nanoparticles: From medicine to energy, *J. Am. Chem. Soc.* **134**, 15607 (2012).
- [7] R. Freeman and I. Willner, Optical molecular sensing with semiconductor quantum dots (QDs), *Chem. Soc. Rev.* **41**, 4067 (2012).
- [8] P. V. Kamat, Boosting the efficiency of quantum dot sensitized solar cells through modulation of interfacial charge transfer, *Acc. Chem. Res.* **45**, 1906 (2012).
- [9] G. H. Carey, A. L. Abdelhady, Z. Ning, S. M. Thon, O. M. Bakr, and E. H. Sargent, Colloidal quantum dot solar cells, *Chem. Rev.* **115**, 12732 (2015).
- [10] E. Lhuillier, M. Scarafagio, P. Hease, B. Nadal, H. Aubin, X. Z. Xu, N. Lequeux, G. Patriarche, S. Ithurria, and B. Dubertret, Infrared photodetection based on colloidal quantum-dot films with high mobility and optical absorption up to THz, *Nano Lett.* **16**, 1282 (2016).
- [11] R. Wang, Y. Shang, P. Kanjanaboos, W. Zhou, Z. Ning, and E. H. Sargent, Colloidal quantum dot ligand engineering for high performance solar cells, *Energy Environ. Sci.* **9**, 1130 (2016).
- [12] D. Loss and D.P. DiVincenzo, Quantum computation with quantum dots, *Phys. Rev. A* **57**, 120 (1998).
- [13] A. Imamoglu, D. D. Awschalom, G. Burkard, D. P. DiVincenzo, D. Loss, M. Sherwin, and A. Small, Quantum Information Processing using Quantum Dot Spins and Cavity QED, *Phys. Rev. Lett.* **83**, 4204 (1999).
- [14] S. Nadj-Perge, S. M. Frolov, E. P. A. M. Bakkers, and L. P. Kouwenhoven, Spin-orbit qubit in a semiconductor nanowire, *Nature (London)* **468**, 1084 (2010).
- [15] Richard J. Warburton, Single spins in self-assembled quantum dots, *Nat. Mater.* **12**, 483 (2013).
- [16] G. Cao, H.-O. Li, G.-D. Yu, B.-Ch. Wang, B.-B. Chen, X.-X. Song, M. Xiao, G.-C. Guo, H.-W. Jiang, X. Hu, and Guo-Ping Guo, Tunable Hybrid Qubit in a GaAs Double Quantum Dot, *Phys. Rev. Lett.* **116**, 086801 (2016).
- [17] M. Kuno, M. Nirmal, M. G. Bawendi, A. Efros, and M. Rosen, Magnetic circular dichroism study of CdSe quantum dots, *J. Chem. Phys.* **108**, 4242 (1998).
- [18] J. A. Gupta, D. D. Awschalom, Al. L. Efros, and A. V. Rodina, Spin dynamics in semiconductor nanocrystals, *Phys. Rev. B* **66**, 125307 (2002).
- [19] H. Htoon, S.A. Crooker, M. Furis, S. Jeong, Al. L. Efros, and V.I. Klimov, Anomalous Circular Polarization of Photoluminescence Spectra of Individual CdSe Nanocrystals in an Applied Magnetic Field, *Phys. Rev. Lett.* **102**, 017402 (2009).

- [20] L. Biadala, Y. Louyer, Ph. Tamarat, and B. Lounis, Band-Edge Exciton Fine Structure of Single CdSe/ZnS Nanocrystals in External Magnetic Fields, *Phys. Rev. Lett.* **105**, 157402 (2010).
- [21] M. J. Fernée, C. Sinito, Y. Louyer, C. Potzner, T. L. Nguyen, P. Mulvaney, P. Tamarat, and B. Lounis, Magneto-optical properties of trions in non-blinking charged nanocrystals reveal an acoustic phonon bottleneck, *Nat. Commun.* **3**, 1287 (2012).
- [22] F. Liu, L. Biadala, A. V. Rodina, D. R. Yakovlev, D. Dunker, C. Javaux, J. P. Hermier, Al. L. Efros, B. Dubertret, and M. Bayer, Spin dynamics of negatively charged excitons in CdSe/CdS colloidal nanocrystals, *Phys. Rev. B* **88**, 035302 (2013).
- [23] E. Johnston-Halperin, D. D. Awschalom, S. A. Crooker, Al. L. Efros, M. Rosen, X. Peng, and A. P. Alivisatos, Spin spectroscopy of dark excitons in CdSe quantum dots to 60 T, *Phys. Rev. B* **63**, 205309 (2001).
- [24] E. L. Ivchenko and A. A. Kiselev, *Fiz. Tekh. Poluprovodn* **26**, 1471 (1992) [*Sov. Phys.-Semicond.* **26**, 827 (1992)].
- [25] A. A. Kiselev, E. L. Ivchenko, and U. Rössler, Electron g factor in one- and zero-dimensional semiconductor nanostructures, *Phys. Rev. B* **58**, 16353 (1998).
- [26] A. V. Rodina, Al. L. Efros, and A. Yu. Alekseev, Effect of the surface on the electron quantum size levels and electron g factor in spherical semiconductor nanocrystals, *Phys. Rev. B* **67**, 155312 (2003).
- [27] I. A. Yugova, A. Grelich, D. R. Yakovlev, A. A. Kiselev, M. Bayer, V. V. Petrov, Yu. K. Dolgikh, D. Reuter, and A. D. Wieck, Universal behavior of the electron g -factor in GaAsAl_xGa_{1-x}As quantum wells, *Phys. Rev. B* **75**, 245302 (2007).
- [28] Joshua Schrier and K.B. Whaley, Tight-binding g factor calculations of CdSe nanostructures, *Phys. Rev. B* **67**, 235301 (2003).
- [29] A. Tadjine, Y.-M. Niquet, and C. Delerue, Universal behavior of electron g -factors in semiconductor nanostructures, *Phys. Rev. B* **95**, 235437 (2017).
- [30] P. Chen and K. B. Whaley, Magneto-optical response of CdSe nanostructures, *Phys. Rev. B* **70**, 045311 (2004).
- [31] L. M. Roth, B. Lax, and S. Zwerdling, Theory of optical magneto-absorption effects in semiconductors, *Phys. Rev.* **114**, 90 (1959).
- [32] C. Hermann and C. Weisbuch, $k \cdot p$ perturbation theory in III-V compounds and alloys: A reexamination, *Phys. Rev. B* **15**, 823 (1977).
- [33] C. Weisbuch and C. Hermann, Optical detection of conduction-electron spin resonance in GaAs, Ga_{1-x}In_xAs, and Ga_{1-x}Al_xAs, *Phys. Rev. B* **15**, 816 (1977).
- [34] O. Z. Karimov, D. Wolverson, J. J. Davies, S. I. Stepanov, T. Ruf, S. V. Ivanov, S. V. Sorokin, C. B. O'Donnell, and K. A. Prior, Electron- g -factor for cubic Zn_{1-x}Cd_xSe determined by spin-flip Raman scattering, *Phys. Rev. B* **62**, 16582 (2000).
- [35] W. W. Piper, II-VI semiconducting compounds, in *International Conference on II-VI Semiconducting Compounds (1967: Brown University)*, edited by D. G. Thomas (W.A. Benjamin, New York, 1967).
- [36] M. Oestreich, S. Hallstein, A. P. Heberle, K. Eberl, E. Bauser, and W. W. Rühle, Temperature and density dependence of the electron Landé factor in semiconductors, *Phys. Rev. B* **53**, 7911 (1996).
- [37] V.K. Kalevich and V.L. Korenev, Electron g -factor anisotropy in asymmetric GaAs/AlGaAs quantum well, *JETP Lett.* **56**, 253 (1992).
- [38] A. A. Sirenko, T. Ruf, M. Cardona, D. R. Yakovlev, W. Ossau, A. Waag, and G. Landwehr, Electron and hole g -factors measured by spin-flip Raman scattering in CdTe/Cd_{1-x}Mg_xTe single quantum wells, *Phys. Rev. B* **56**, 2114 (1997).
- [39] J. van Bree, A. Yu. Silov, P. M. Koenraad, and M. E. Flatté, Spin-Orbit-Induced Circulating Currents in a Semiconductor Nanostructure, *Phys. Rev. Lett.* **112**, 187201 (2014).
- [40] C. E. Pryor and M. E. Flatté, Landé g Factors and Orbital Momentum Quenching in Semiconductor Quantum Dots, *Phys. Rev. Lett.* **96**, 026804 (2006).
- [41] D. Csontos, P. Brusheim, U. Zülicke, and H. Q. Xu, Spin-3/2 physics of semiconductor hole nanowires: Valence-band mixing and tunable interplay between bulk-material and orbital bound-state spin splittings, *Phys. Rev. B* **79**, 155323 (2009).
- [42] M. A. Semina and R. A. Suris, Holes localized in nanostructures in an external magnetic field: g -factor and mixing of states, *Semiconductors* **49**, 797 (2015).
- [43] M. A. Semina, A. A. Golovatenko, and A. V. Rodina, Ground state of the holes localized in II-VI quantum dots with Gaussian potential profiles, *Phys. Rev. B* **93**, 045409 (2016).
- [44] Al. L. Efros, M. Rosen, M. Kuno, M. Nirmal, D.J. Norris, and M. Bawendi, Band-edge exciton in quantum dots of semiconductors with a degenerate valence band: Dark and bright exciton states, *Phys. Rev. B* **54**, 4843 (1996).
- [45] A. A. Kiselev and L. V. Moiseev, Zeeman splitting of heavy-hole states in III-V and II-VI heterostructures, *Fiz. Tverd. Tela* **38**, 1574 (1996) [*Phys. Solid State* **38**, 866 (1996)].
- [46] R. Kotlyar, T. L. Reinecke, M. Bayer, and A. Forchel, Zeeman spin splittings in semiconductor nanostructures, *Phys. Rev. B* **63**, 085310 (2001).
- [47] M. J. Snelling, E. Blackwood, C. J. McDonagh, R. T. Harley, and C. T. B. Foxon, Exciton, heavy-hole, and electron g factors in type-I GaAs/Al_xGa_{1-x}As quantum wells, *Phys. Rev. B* **45**, 3922 (1992).
- [48] J. van Bree, A. Yu. Silov, P. M. Koenraad, M. E. Flatté, and C. E. Pryor, g factors and diamagnetic coefficients of electrons, holes, and excitons in InAs/InP quantum dots, *Phys. Rev. B* **85**, 165323 (2012).
- [49] G. L. Bir and G. E. Pikus, *Symmetry and Strain-Induced Effects in Semiconductors* (Wiley, New York, 1974).
- [50] A. V. Rodina, M. Dietrich, A. Göldner, L. Eckey, A. Hoffmann, Al. L. Efros, M. Rosen, and B. K. Meyer, Free excitons in wurtzite GaN, *Phys. Rev. B* **64**, 115204 (2001).
- [51] J. M. Luttinger, Quantum theory of cyclotron resonance in semiconductors: general theory, *Phys. Rev.* **102**, 1030 (1956).
- [52] B. L. Gel'mont and M. I. D'yakonov, Acceptor levels in diamond-type semiconductors, *Fiz. Tekh. Poluprovodn* **5**, 2191 (1971) [*Sov. Phys.-Semicond.* **5**, 1905 (1971)].
- [53] B. L. Gel'mont and M. I. D'yakonov, g -factor of acceptors in semiconductors with the diamond structure, *Fiz. Tekh. Poluprovodn* **7**, 2013 (1973) [*Sov. Phys. Semicond.* **7**, 1345 (1973)].
- [54] Al. L. Efros, Fine Structure and Polarization Properties of Band-Edge Excitons in Semiconductor Nanocrystals; Chapter 3, in *Semiconductor and Metal Nanocrystals: Synthesis and Electronic and Optical Properties*, edited by V. I. Klimov (M. Dekker, New York, 2003), pp. 103–141.

- [55] E. V. Shornikova, A. A. Golovatenko, D. R. Yakovlev, A. V. Rodina, L. Biadala, G. Qiang, A. Kuntzmann, M. Nasilowski, B. Dubertret, A. P. I. Moreels, and M. Bayer, Surface spin magnetism controls the polarized exciton emission from CdSe nanoplatelets, *Nat. Nanotechnol.* **15**, 277 (2020).
- [56] E. Shornikova, D. Yakovlev, L. Biadala, S. Crooker, V. Belykh, M. Kochiev, A. Kuntzmann, M. Nasilowski, B. Dubertret, and M. Bayer, Negatively charged excitons in cdse nanoplatelets, *Nano Lett.* **20**, 1370 (2020).
- [57] E. Shornikova, D. Yakovlev, D. Tolmachev, V. Ivanov, I. Kalitukha, Victor Sapega, D. Kudlacik, Y. Kusrayev, A. Golovatenko, S. Shendre, S. Delikanli, H. Demir, and M. Bayer, Magneto-optics of excitons interacting with magnetic ions in cdse/cdmns colloidal nanoplatelets, *ACS Nano* **14**, 9032 (2020).
- [58] M. V. Durnev, M. M. Glazov, and E. L. Ivchenko, Giant zeeman splitting of light holes in GaAs/AlGaAs quantum wells, *Phys. E (Amsterdam)* **44**, 797 (2012).
- [59] H. W. van Kesteren, E. C. Cosman, W. A. J. A. van der Poel, and C. T. Foxon, Fine structure of excitons in type-II GaAs/AlAs quantum wells, *Phys. Rev. B* **41**, 5283 (1990).
- [60] X. Marie, T. Amand, P. Le Jeune, M. Paillard, P. Renucci, L. E. Golub, V. D. Dymnikov, and E. L. Ivchenko, Hole spin quantum beats in quantum-well structures, *Phys. Rev. B* **60**, 5811 (1999).
- [61] K. J. Vahala and P. C. Sercel, Application of a Total-Angular-Momentum Basis to Quantum-Dot Band Structure, *Phys. Rev. Lett.* **65**, 239 (1990).
- [62] P. C. Sercel and K. J. Vahala, Analytical formalism for determining quantum-wire and quantum-dot band structure in the multiband envelope-function approximation, *Phys. Rev. B* **42**, 3690 (1990).
- [63] A. Baldereschi and N. O. Lipari, Spherical model of shallow acceptor states in semiconductors, *Phys. Rev. B* **8**, 2697 (1973).
- [64] L. G. C. Rego, P. Hawrylak, J. A. Brum, and A. Wojs, Interacting valence holes in p-type SiGe quantum disks in a magnetic field, *Phys. Rev. B* **55**, 15694 (1997).
- [65] D. A. Broido and L. J. Sham, Effective masses of holes at gaas-algaas heterojunctions, *Phys. Rev. B* **31**, 888 (1985).
- [66] A. I. Ekimov, F. Hache, M. C. Schanne-Klein, D. Ricard, Ch. Flytzanis, I. A. Kudryavtsev, T. V. Yazeva, A. V. Rodina, and Al. L. Efros, Absorption and intensity-dependent photoluminescence measurements on CdSe quantum dots: assignment of the first electronic transitions, *J. Opt. Soc. Am. B* **10**, 100 (1993).
- [67] A. R. Edmonds, *Angular Momentum in Quantum Mechanics* (Princeton University Press, Princeton, NJ, 1957).
- [68] Calvin Yi-Ping Chao and Shun Lien Chuang, Spin-orbit-coupling effects on the valence-band structure of strained semiconductor quantum wells, *Phys. Rev. B* **46**, 4110 (1992).
- [69] A. A. Golovatenko, M. A. Semina, A. V. Rodina, and T. V. Shubina, Excitons and biexcitons in spheroidal quantum dots A_2B_6 , *Phys. Solis State* **60**, 1510 (2018).
- [70] G. B. Grigoryan, E. M. Kazarayn, Al. L. Efros, and T. V. Yazeva, Hole quantization and absorption-edge in spherical microcrystals of semiconductors with complex valence band structure, *Fiz. Tverd. Tela* **32**, 1772 (1990) [*Sov. Phys.-Solid State* **32**, 1031 (1990)].
- [71] Al. L. Efros, Luminescence polarization of cdse microcrystals, *Phys. Rev. B* **46**, 7448 (1992).
- [72] Al. L. Efros and A. V. Rodina, Band-edge absorption and luminescence of nonspherical nanometer-size crystals, *Phys. Rev. B* **47**, 10005 (1993).
- [73] A. Baldereschi and Nunzio O. Lipari, Cubic contributions to the spherical model of shallow acceptor states, *Phys. Rev. B* **9**, 1525 (1974).
- [74] Sadao Adachi, *Handbook on Physical Properties of Semiconductors* (Springer, New York, 2004).
- [75] S. Zh. Karazhanov, Ab initio studies of the band parameters of III-v and II-vi zinc-blende semiconductors, *Semiconductors* **39**, 161 (2005).
- [76] H. Fu, L.-W. Wang, and A. Zunger, Applicability of the k-p method to the electronic structure of quantum dots, *Phys. Rev. B* **57**, 9971 (1998).
- [77] D.J. Norris, Al. L. Efros, M. Rosen, and M.G. Bawendi, Size dependence of exciton fine structure in CdSe quantum dots, *Phys. Rev. B* **53**, 16347 (1996).
- [78] A. B. Kapustina, B. V. Petrov, A. V. Rodina, and R. P. Seisyan, Magnetic absorption of hexagonal crystals CdSe in strong and weak fields: Quasi-cubic approximation, *Phys. Solid State* **42**, 1242 (2000).
- [79] J. Berezovsky, M. Ouyang, F. Meier, D. D. Awschalom, D. Battaglia, and X. Peng, Spin dynamics and level structure of quantum-dot quantum wells, *Phys. Rev. B* **71**, 081309(R) (2005).
- [80] W. Hackenberg, R. T. Phillips, and H. P. Hughes, Investigation of the luttinger parameters for inp using hot-electron luminescence, *Phys. Rev. B* **50**, 10598 (1994).
- [81] S. I. Kohanovskii, Yu. M. Makushenko, R. P. Seisyan, Al. L. Efros, T. V. Yazeva, M. A. Abdullaev, Quasi-landau oscillating magnetoabsorption of InP exciton rydberg states in an intermediate magnetic field, *Fiz. Tverd. Tela* **33**, 1719 (1991) [*Sov. Phys.-Solid State* **33**, 967 (1991)].
- [82] N. O. Lipari and A. Baldereschi, Angular Momentum Theory and Localized States in Solids. Investigation of Shallow Acceptor States in Semiconductors, *Phys. Rev. Lett.* **25**, 1660 (1970).
- [83] A. V. Rodina and Al. L. Efros, Band-edge biexciton in nanocrystals of semiconductors with a degenerate valence band, *Phys. Rev. B* **82**, 125324 (2010).
- [84] S. Ithurria, M. D. Tessier, B. Mahler, R. P. S. M. Lobo, B. Dubertret and Al. L. Efros, Colloidal nanoplatelets with two-dimensional electronic structure, *Nat. Mater.* **10**, 936 (2011).
- [85] E. V. Shornikova, L. Biadala, D. R. Yakovlev, V. F. Sapega, Y. G. Kusrayev, A. A. Mitioglu, M. V. Ballottin, P. C. M. Christianen, V. V. Belykh, M. V. Kochiev, N. N. Sibeldin, A. A. Golovatenko, A. V. Rodina, N. A. Gippius, A. Kuntzmann, Y. Jiang, M. Nasilowski, B. Dubertret, and M. Bayer, Addressing the exciton fine structure in colloidal nanocrystals: the case of CdSe nanoplatelets, *Nanoscale* **10**, 646 (2018).
- [86] Th. Wimbauer, K. Oettinger, Al. L. Efros, B. K. Meyer, and H. Brugger, Zeeman splitting of the excitonic recombination in $In_xGa_{1-x}As/GaAs$ single quantum wells, *Phys. Rev. B* **50**, 8889 (1994).
- [87] S. Christodoulou, J. I. Climente, J. Planelles, R. Brescia, M. Prato, B. Martín-García, A. H. Khan, and I. Moreels,

- Chloride-Induced Thickness Control in CdSe Nanoplatelets, *Nano Lett.* **18**, 6248 (2018).
- [88] B. Ji, E. Rabani, Al. L. Efros, R. Vaxenburg, O. Ashkenazi, D. Azulay, U. Banin, and O. Millo, Dielectric Confinement and Excitonic Effects in Two-Dimensional Nanoplatelets, *ACS Nano* **14**, 8257 (2020).
- [89] M. Olutas, B. K. Guzelurk, Y. Kelestemur, A. Yeltik, S. Delikanli, and H. V. Demir, Lateral size-dependent spontaneous and stimulated emission properties in colloidal cdse nanoplatelets, *ACS Nano* **9**, 5041 (2015).
- [90] S. Ayari, M. T. Quick, N. Owschimikow, S. Christodoulou, G. H. V. Bertrand, M. Artemyev, I. Moreels, U. Woggon, S. Jaziri, and Alexander W. Achtstein, Tuning trion binding energy and oscillator strength in a laterally finite 2D system: CdSe nanoplatelets as a model system for trion properties, *Nanoscale* **12**, 14448 (2020).
- [91] P. Pfeffer and W. Zawadzki, Five-level-k-model for the conduction and valence bands of GaAs and InP, *Phys. Rev. B* **53**, 12813 (1996).
- [92] Al. L. Efros and M. Rosen, Quantum size level structure of narrow-gap semiconductor nanocrystals: Effect of band coupling, *Phys. Rev. B* **58**, 7120 (1998).
- [93] S. Kapoor, J. Kumar, and P.K. Sen, Magneto-optical analysis of anisotropic CdZnSe quantum dots, *Phys. E (Amsterdam)* **42**, 2380 (2010).
- [94] N. J. Traynor, R. T. Harley, and R. J. Warburton, Zeeman splitting and g factor of heavy-hole excitons in $\text{In}_x\text{Ga}_{1-x}\text{As}/\text{GaAs}$ quantum wells, *Phys. Rev. B* **51**, 7361 (1995).
- [95] J. Jadczyk, M. Kubisa, K. Ryczko, L. Bryja, and M. Potemski, High magnetic field spin splitting of excitons in asymmetric GaAs quantum wells, *Phys. Rev. B* **86**, 245401 (2012).
- [96] P. E. Faria Junior, T. Campos, C. M. O. Bastos, M. Gmitra, J. Fabian, and G. M. Sipahi, Realistic multiband $k \cdot p$ approach from ab initio and spin-orbit coupling effects of InAs and InP in wurtzite phase, *Phys. Rev. B* **93**, 235204 (2016).
- [97] P. E. Faria Junior, D. Tedeschi, M. De Luca, B. Scharf, A. Polimeni, and J. Fabian, Common nonlinear features and spin-orbit coupling effects in the Zeeman splitting of novel wurtzite materials, *Phys. Rev. B* **99**, 195205 (2019).
- [98] D. Kudlacik, V. F. Sapega, D. R. Yakovlev, I. V. Kalitukha, E. V. Shornikova, A. V. Rodina, E. L. Ivchenko, G. S. Dimitriev, M. Nasilowski, B. Dubertret, and M. Bayer, Single and double electron spin-flip raman scattering in CdSe colloidal nanoplatelets, *Nano Lett.* **20**, 517 (2019).
- [99] R. Hu, D. R. Yakovlev, P. Liang, G. Qiang, C. Chen, T. Jia, Zh. Sun, M. Bayer, and D. Feng, Origin of two larmor frequencies in the coherent spin dynamics of colloidal CdSe quantum dots revealed by controlled charging, *J. Phys. Chem. Lett.* **10**, 3681 (2019).
- [100] Z. Wu, Y. Zhang, R. Hu, M. Jiang, P. Liang, Q. Yang, L. Deng, T. Jia, Z. Sun, and D. Feng, Hole-Acceptor-Manipulated Electron Spin Dynamics in CdSe Colloidal Quantum Dots, *J. Phys. Chem. Lett.* **12**, 2126 (2021).
- [101] N. P. Stern, M. Poggio, M. H. Bartl, E. L. Hu, G. D. Stucky, and D. D. Awschalom, Spin dynamics in electrochemically charged CdSe quantum dots, *Phys. Rev. B* **72**, 161303(R) (2005).
- [102] E. V. Shornikova, L. Biadala, D. R. Yakovlev, D. Feng, V. F. Sapega, N. Flipo, A. A. Golovatenko, M. A. Semina, A. V. Rodina, A. A. Mitioglu, M. V. Ballottin, P. C. M. Christianen, Y. G. Kusrayev, M. Nasilowski, B. Dubertret, and M. Bayer, Electron and hole g -factors and spin dynamics of negatively charged excitons in CdSe/CdS colloidal nanoplatelets with thick shells, *Nano Lett.* **18**, 373 (2018).
- [103] A. Granados del Aguila, G. Pettinari, E. Groeneveld, C. de Mello Donega, D. Vanmaekelbergh, J. C. Maan, and P. C. M. Christianen, Optical Spectroscopy of Dark and Bright Excitons in CdSe Nanocrystals in High Magnetic Fields, *J. Phys. Chem. C* **121**, 23693 (2017).
- [104] G. Qiang, A. A. Golovatenko, E. V. Shornikova, D. R. Yakovlev, A. V. Rodina, E. A. Zhukov, I. V. Kalitukha, V. F. Sapega, V. Kh. Kaibyshev, M. A. Prosnikov, P. C. M. Christianen, A. A. Onushchenko, and M. Bayer, Polarized emission of CdSe nanocrystals in magnetic field: The role of phonon-assisted recombination of the dark exciton, *Nanoscale* **13**, 790 (2021).
- [105] S. I. A. Brumberg, S. M. Harvey, J. P. Philbin, B. T. Diroll, B. Lee, S. A. Crooker, M. R. Wasielewski, E. Rabani, and R. D. Schaller, Determination of the in-plane exciton radius in 2D CdSe nanoplatelets via magneto-optical spectroscopy, *ACS Nano* **13**, 8589 (2019).
- [106] M. Furis, H. Htoon, M.A. Petruska, V.I. Klimov, T. Barrick, and S.A. Crooker, Bright-exciton fine structure and anisotropic exchange in CdSe nanocrystal quantum dots, *Phys. Rev. B* **73**, 241313(R) (2006).
- [107] F. J. P. Wijnen, J. H. Blokland, P. T. K. Chin, P. C. M. Christianen, and J. C. Maan, Competition between zero-phonon and phonon-assisted luminescence in colloidal CdSe quantum dots, *Phys. Rev. B* **78**, 235318 (2008).
- [108] A. Brodu, V. Chandrasekaran, L. Scarpelli, J. Buhot, F. Masia, M. V. Ballottin, M. Severijnen, M. D. Tessier, D. Dupont, F. T. Rabouw, P. C. M. Christianen, C. de Mello Donega, D. Vanmaekelbergh, W. Langbein, and Z. Hens, Fine structure of nearly isotropic bright excitons in InP/ZnSe colloidal quantum dots, *J. Phys. Chem. Lett.* **10**, 5468 (2019).
- [109] E.L. Ivchenko, A.A. Kiselev, and M. Willander, Electronic g factor in biased quantum wells, *Solid State Commun.* **102**, 375 (1996).
- [110] I. A. Merkulov and A. V. Rodina, Exchange interaction between carriers and magnetic ions in quantum size heterostructures, in *Introduction to the Physics of Diluted Magnetic Semiconductors*, edited by J. Kossut and J. A. Gaj (Springer, Berlin, 2010), Chap. 3, pp. 65–101.
- [111] A. V. Rodina and A. Yu. Alekseev, Theory of intrinsic electric polarization and spin Hall current in spin-orbit-coupled semiconductor heterostructures, *Phys. Rev. B* **78**, 115304 (2008).
- [112] R. Benchamekh, N. A. Gippius, J. Even, M. O. Nestoklon, J.-M. Jancu, S. Ithurria, B. Dubertret, Al. L. Efros, and P. Voisin, Tight-binding calculations of image-charge effects in colloidal nanoscale platelets of CdSe, *Phys. Rev. B* **89**, 035307 (2014).
- [113] Sadao Adachi, *Properties of Group-IV, III-V and II-VI Semiconductors* (Wiley, Hoboken, NJ, 2005).
- [114] Z. Zhang, Z. Jin, H. Ma, Y. Xu, X. Lin, G. Ma, and X. Sun, Room-temperature spin coherence in zinc blende CdSe quantum dots studied by time-resolved faraday ellipticity, *Phys. E (Amsterdam)* **56**, 85 (2014).
- [115] A. V. Rodina and E. L. Ivchenko, Theory of single and double electron spin-flip raman scattering in semiconductor nanoplatelets, *Phys. Rev. B* **102**, 235432 (2020).